Ion mobility spectrometry-mass spectrometry (IMS-MS) of small molecules: separating and assigning structures to ions

Cris Lapthorn, Frank Pullen* and Babur Z. Chowdhry
University of Greenwich, School of Science, Medway Campus, Chatham, Kent ME4 4TB, UK
Frank.Pullen@greenwich.ac.uk

ACCEPTED FOR PUBLICATION

This is the peer reviewed version of the following article: C. Lapthorn, F. Pullen, and B. Z. Chowdhry, "Ion mobility spectrometry-mass spectrometry (IMS-MS) of small molecules: Separating and assigning structures to ions," Mass Spectrometry Reviews, vol. 32, no. 1, pp. 43–71, 2013 which has been published in final form at http://dx.doi.org/10.1002/mas.21349

(ABSTRACT)

The phenomenon of ion mobility (IM), the movement/transport of charged particles under the influence of an electric field, was first observed in the early twentieth Century and harnessed later in ion mobility spectrometry (IMS). There have been rapid advances in instrumental design, experimental methods and theory together with contributions from computational chemistry and gas-phase ion chemistry which have diversified the range of potential applications of contemporary IMS techniques. Whilst IMS-mass spectrometry (IMS-MS) has recently been recognized for having significant research/applied industrial potential and encompasses multi-/cross-disciplinary areas of science, the applications and impact from decades of research are only now beginning to be utilised for 'small molecule' species. This review focuses on the application of IMS-MS to 'small molecule' species typically used in drug discovery (from 100 to 500 Da) including an assessment of the limitations and possibilities of the technique. Potential future developments in instrumental design, experimental methods and applications are addressed.

The typical application of IMS-MS in relation to small molecules has been to separate species in fairly uniform molecular classes such as mixture analysis, including metabolites. Separation of similar species has historically been challenging using IMS as the resolving power, R, has been low (from 3-100) and the differences in collision cross-sections that could be measured have been relatively small, so instrument and method development has often focused on increasing resolving power. However, IMS-MS has a range of other potential applications that are examined in this review where it displays unique advantages, including: determination of small molecule structure from drift time, 'small molecule' separation in achiral and chiral mixtures, improvement in selectivity, identification of carbohydrate isomers, metabonomics, and for understanding the size and shape of small molecules. This review provides a broad but selective overview of current literature, concentrating on IMS-MS, not solely IMS, and small molecule applications.

Keywords: ion-mobility mass spectrometry; ion mobility spectrometry; mass spectrometry; small molecule; mass-mobility correlation; collision cross-section; ion mobility; FAIMS; drift-time; travelling wave; structural; computational; differential mobility spectrometry; differential mobility analyzer

I. INTRODUCTION TO IMS

The existence of ions in the gas-phase was first discovered when investigating changes in the electrical conductance of air (Thomson, 1903) which had previously been thought to be an electrical insulator. Further work established the generation of ions by UV and X-ray from work by Thomson and Rutherford (1896), Roentgen (1896) and Rutherford (1897)). The rudimentary scientific tools available at the time did not allow a comprehensive understanding of ion behaviour but the behaviour of simple gas-phase ions in a weak electric field was further elucidated by Langevin (1905), who demonstrated

that air was a mixture of gases and developed models that described these simpler systems remarkably well.

Thomson and Aston later developed the first mass spectrometer (Aston, 1919) and further research focussed on low pressure studies of ion-molecule systems that, although not directly involving typical ion mobility pressure regimes, accrued knowledge in the behaviour of ion motion in a partial vacuum.

The rapid uptake of IMS in military and forensic applications (Zolotov, 2006) benefited from the relatively high proton affinity of the analytes (chemical warfare agents, explosives and illicit drugs), low detection limits and miniaturisation of IMS instrumentation. IMS instrumentation was re-designed for the field, used internal calibrant standards and simplified user interfaces allowed their use by non-scientist military and security personnel. IMS instrumentation is now ubiquitous in handheld forensics, cleaning validation and military applications (from border control to explosive testing in war zones).

Separation in IMS occurs rapidly, in milliseconds, rather than seconds as in chromatography, so IMS is now beginning to be recognised as a powerful separation step which can be utilised post-ionisation using a range of equipment, benefits from robust day-to-day operation and allows size and shape separation and measurement of analytes that cannot easily be derived using other techniques. Miniaturisation, demonstrated so far primarily in overtone IMS and microfabricated Field Asymmetric IMS (FAIMS), is a highly attractive feature and IMS typically has a low detection limit of nanograms and does not require expensive and environmentally damaging solvents.

II. INTRODUCTION TO IMS-MS

The most important aspect of the combination of an IMS separation (typically occurring in the millisecond time-frame) and MS detection (typically occuring in the microsecond time-frame) is that it allows an additional separation step to be obtained on a MS time-frame (e.g. in addition to liquid chromatography), without compromising the speed of MS detection.

The work of McDaniel and Martin (1960), Kebarle (1965) and Hogg (1965), Albritton et al., (1968) and later Crompton and Milloy (1977) developed the recognizable configuration of linear drift-tube IMS (DT-IMS). The combination of ion mobility and mass spectrometry allowed more complex studies to be conducted in order to develop models of ion mobility.

IMS was first hyphenated to a mass spectrometer by Barnes, McDaniel and Martin (1961) using a magnetic sector mass spectrometer; subsequently McAffee and Edelson (1963) described hyphenation to a time-of-flight (TOF) MS. The coupling of IMS with a TOF mass spectrometer is particularly appropriate because the TOF mass spectrometer has the fastest data acquisition rate of any mass spectrometer and can acquire many spectra on the microsecond scale whilst the IMS analytes arrive on a millisecond timescale.

A review by Hill et al. (2007) describes the early development of IMS-MS with significant contributions and discoveries including those from Bowers, Kemper, Clemmer and Kebarle. IMS has since been interfaced to quadrupole mass spectrometers (Karasek et al., 1976; Wu et al., 1998), quadrupole ion traps (Creaser et al., 2000), linear ion traps and Fourier-transform ion cyclotron mass spectrometers (Bluhm et al., 2000) which is beneficial in terms of a wider linear dynamic range and increased mass spectral resolution. Clemmer et al., (1997) and Creaser et al., (2000) also reversed the stages to produce a MS-IMS design that traps and stores ions in an initial quadrupole ion trap for subsequent ion mobility measurements which has the advantage of pre-concentrating low abundant components.

Recently IMS has been hyphenated to mass spectrometry systems and the availability of commercially supported instrumentation has arguably led to a rapid increase in the number of publications on IMS-MS, as shown in FIGURE 1. FAIMS, a type of differential mobility spectrometry, originated in Russia in the early 1980s (Gorshkov, 1982) emerged as an analytical tool (Buryakov et al., 1993), and was later commercialised by Ionalytics (Selectra, 2003), as a front-end accessory for MDS Sciex (Concord, Ontario, Canada) mass spectrometer systems (2004), Thermo FAIMS, (2007) and Owlstone Nanotechnologies FAIMS. Waters Inc. (Milford, MA) launched the first generation Synapt Triwave travelling wave IMS system in 2006 and updated with a second generation instrument with improved resolution (G2, 2009) and improvements to sensitivity (G2S, 2011). AB Sciex launched the

SelexION ion mobility device in 2011 for their triple quadrupole mass spectrometer and quadrupole-trap mass spectrometer.

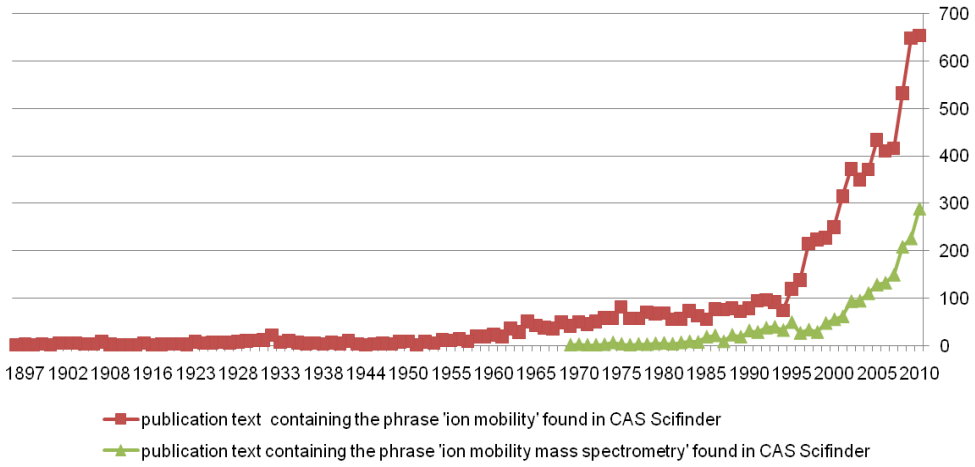

***FIGURE* 1.** Chart showing number of publications containing the phrases "ion mobility" and "ion mobility mass spectrometry" obtained using CAS Scifinder.

There has been limited recognition of the potential of IMS-MS analysis for 'rule-of-5' type small-molecules (Lipinski et al., 1997) outside of traditional IMS analyte classes (e.g. explosives, chemical warfare and illicit drugs). The historical lack of interest and sporadic periods of development in IMS-MS for small molecule applications seems most likely to be due to perceived poor resolution, strengths in competing chromatographic techniques and weaknesses in the robustness of IMS regarding a poor linear range (Turner and Brokenshire, 1994), "memory effects" from contamination (Gehrke, 2001) and interference from matrices.

In contrast IMS-MS has been applied to biomolecules including peptides (Harvey, Macphee & Barran , 2011), proteins (60 kDa-150 kDa) and large protein complexes (1- 4 MDa) (Uetrecht et al., 2010) particularly after the application of non-covalent mass spectrometry conditions to IMS-MS. Using these especially gentle electrospray ionisation conditions is believed to maintain the weak (cooperative) molecular interactions present in many biomolecular structures and thus avoid fragmentation. Whilst IMS-MS typically lacks the resolution (1% error or 10 nm^2) of x-ray or NMR for large molecular weight biomolecules it enables analysis using smaller amount of material, allows analysis of structures >100 kDa that are difficult to analyse by NMR and is, arguably, as realistic an environment as x-ray structures due to lattice effects present. IMS-MS has, therefore, been utilised as a tool to probe the stabilisation of proteins in the presence of ligands and metals (as a unique method of metal speciation; Souza Pessôa et al., 2011), protein-protein-interactions, protein mutants and their structural consequences as well as protein unfolding via various means of ion activation (Jurneczko and Barran, 2011). In addition to detailed understanding of individual biomolecular systems, IMS-MS has also been applied to more high-throughput analytical approaches including screening of phosphorylated peptides (Thalassinos et al., 2009), identification and separation of chemically cross-linked peptides (Santos et al., 2010) and combining topology in protein substructures with proteomics data (Zhou and Robinson, 2010). This review does not attempt to summarise biomolecule analysis by IMS-MS, which is covered by many authors, but rather to contrast the adoption of IMS-MS in biomolecule analysis and focuses on small molecule applications.

III. DIFFERENCES IN PERFORMANCE OF IMS-MS AND IMS

A. The ion efficiency and resolution challenge

Some of the key differences between IMS and hyphenated IMS-MS include the pressure regime in the ion mobility cell, the size of the instrument and the typical ionisation source. Whilst specifications and performance in IMS may be indicative of those in IMS-MS there are some technical reasons why this may not follow. It is critical to note that the results may well be different in IMS-MS compared to IMS especially due to sensitivity issues and pressure regime changes from IMS to MS stages.

In IMS-MS there are often two main challenges (i) to utilise all the ions from the ionisation source, (especially in a pulsed IMS separation such as drift-time IMS, but not a challenge in DMS or FAIMS which typically have a 100% duty cycle if a single transmission voltage is selected) and (ii) elimination of all neutral species whilst ensuring transmission of ions to the MS stages to maintain sensitivity. Traditionally DT-IMS-MS sensitivity has been estimated to be inversely proportional to the IMS resolving power squared; ion losses at the IMS exit aperture ranging from 99 to 99.9% (Tang et al., 2005) and ion introduction losses being between 99.6 to 99.9% (Belov et al., 2008). The desire to increase the gas pressure in the DT-IMS cell to increase resolution must therefore be balanced with the possibility that it may well reduce ion transmission by requiring a reduction of the aperture size in the interface from IMS to MS. The different pressure regimes in IMS systems are described in Table 1.

For DT-IMS-MS the drift gas pressure must be increased proportionally to electric field strength in order to maintain a low E/N ratio (<2 x 10^{-17} Vcm^2), required to obtain field-independent mobilities for which the simplified Mason-Schamp equation (Mason and McDaniel, 1988) holds:

$$K = (3q/16N)(2\pi/\mu kT)^{1/2} 1/\Omega \qquad (1)$$

Where *K* is the ion mobility, q is the ionic charge, N is the buffer gas density, μ is the reduced mass of the buffer gas and the ion, k is the Boltzman constant, T is the temperature and Ω is the collision cross-section (CCS).

For Travelling Wave Ion Mobility-MS (TWIMS-MS) the gas pressure must also be increased proportionally to the electric field, such that:

$$K = K_o N_o / N = K P_o T / (P T_o) \qquad (2)$$

where K is the ion mobility, N is the buffer gas density, N_o is the Loschmidt number (the value of *N* at standard temperature (T_o = 273K) and pressure (P = 1 Atm) and K_o is the reduced ion mobility.

TABLE 1. Pressure regimes in typical IMS systems.

Type of IMS system	Pressure regime	Typical operating pressure
Ambient DT-IMS	Ambient pressure	1000 mbar (Kanu et al., 2008)
Reduced pressure DT-IMS	Reduced pressure	10^{-5} (Ruotolo et al., 2002b) to 1.3 (Valentine et al., 2001) mbar
FAIMS or DMS	Ambient pressure->ambient pressure	400 to 1571 mbar (Kolakowski and Mester, 2007)
Travelling wave IMS	Reduced pressure	0.5 mbar (Waters Synapt G1) to >3 mbar (Waters Synapt G2) (Giles et al., 2011)
Differential mobility analysis	Ambient pressure	1013 mbar

Approaches to maximise sensitivity include utilising quadrupole and octopole ion traps (Henderson et al., 1999;Creaser et al., 2000; Myung et al., 2003) and electrodynamic ion funnels (Wyttenbach et al., 2001) to accumulate and introduce ions efficiently from the ion source to increase the sensitivity of DT-IMS. Multiplexing approaches including Hadamard (Clowers et al., 2006) and Fourier-type (Tarver, 2004) gating techniques have also been utilised for increasing the sensitivity of DTIMS, by increasing the frequency of ion injection events and thus increasing the quantity of ions injected into DT-IMS by up to 50%. Most of these approaches have been integrated into full IMS-MS systems with dramatic improvements in sensitivity.

There is some uncertainty in the identification of the ions in their transmission through the IM cell and it seems clear that hyphenating IMS and MS allows a more comprehensive understanding of the

ionisation processes and fragmentation pathways in IMS. For example, when using a radioactive ^{63}Ni cell, proton transfer to the analytes should lead to protonated monomer and dimer ions; however, without a mass spectrometer as the detector, the identification of the ions in the ion cell cannot be unambiguously ascertained. Indeed, a comparison of limonene and 2-nonanone by IMS and IMS-MS resulted in a variety of unexpected fragments and ions, resulting in a non-trivial IMS spectrum and making interpretation of the results difficult (Vautz et al., 2010). Any unambiguous identification of ions in IMS will be important both in structural measurements (size, shape and topology) and for comparison of related IMS techniques (e.g. TWIMS-MS) that often use historical DT-IMS-MS data as calibration standards in ion mobility and collision cross-section calculations.

B. Features of IMS techniques utilised in IMS-MS

IMS-MS potentially provides a number of advantages over and above IMS including:

i) as a rapid gas-phase separation step before mass spectrometryanalysis,
ii) the identification of ions subsequent to characteristic drift times by comparison with data acquired under comparable conditions,
iii) measurements of collision cross-sections and derivation of further information about size and shape, either by comparison with computational modeling or by analysis within a series of compounds
iv) better characterisation of ion and ion-neutral ion mobilities by simultaneous acquisition of mass spectrometry data, and
v) better characterisation of ionisation (Tang et al., 2006) and fragmentation pathways via a better understanding of gas-phase ion structures

IMS has been hyphenated to liquid chromatography, gas chromatography (Baim and Hill, 1982; Snyder et al., 1993), super-critical fluid chromatography (Eatherton et al., 1986; Huang et al., 1991), ions produced via matrix assisted laser desorption ionisation (Jackson et al., 2007), desorption electrospray ionisation (Weston et al., 2005), pulsed corona discharge ionisation (Hill and Thomas, 2003) and miniaturised to microchip scale (Shvartsburg et al., 2009b).

IMS-MS systems are typically composed of four stages (Figure 2):

1) an ion source e.g. MALDI or electrospray that generates ions. Electrospray ion sources have been preferred for retaining native-like structures in biological systems.
2) an IMS cell, where charged particles migrate under the influence of an electric field.
3) a mass analyzer, typically a time-of-flight (TOF) mass spectrometer which is designed to allow a fast acquisition rate and large mass detection range.
4) an ion detector.

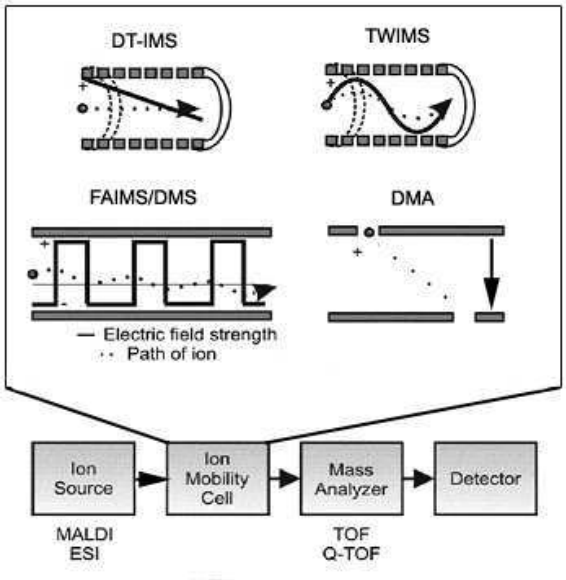

***FIGURE* 2.** Overview of typical ion-mobility mass spectrometer configurations, adapted from Enders and Mclean, 2009.

There are four main types of IM cell utilised in IMS-MS.

(i) Drift-time IMS (DT-IMS) is the simplest configuration where collision cross-section (CCS) can be directly calculated without calibration and provides the highest resolving power. A tube is filled with a buffer gas (or mixture) and a low voltage field is applied, typically from 5 to 100 Vcm^{-1}. The ions collide with neutral buffer gas molecules, exit via a detector and the collision cross-section Ω_T, at a temperature T can be obtained by measuring the velocity of the ions and solving the Mason-Schamp equations at intermediate electrical fields (5-100 Vcm^{-1}):

$$V_d = KE \tag{3}$$

where V_d is the drift velocity of the ion, K is the ion mobility, E is the imposed electric field, and

$$\Omega_T = \left(\frac{3ze}{16N}\right)\left(\frac{2\pi}{\mu kT}\right)^{1/2}\left(\frac{1}{K}\right) \tag{4}$$

where z is the numerical charge, e is the elementary charge, N is the number density of the buffer gas, μ is the reduced mass of the ion- buffer gas neutral pair, k is the Boltzmann constant and T the temperature in Kelvin.

DT-IMS suffers from an inherent lack of sensitivity, due to a pulsed analysis (where ions are measured in packets), and the subsequent loss in duty cycle, as the time between packets of ions is not utilised. A review of IMS by Eiceman and Karpas (2004) discusses the history of IMS, the chemistry and physics of ion behaviour and reflects on the potential future development and applications of IMS.

In linear DT-IMS, illustrated in FIGURE 3, the sample is introduced to an ionisation region where ionisation can take place by a number of methods including β-emission from a ^{63}Ni corona discharge, photo-ionisation, electrospray etc. Ions are allowed through an electric shutter grid, whilst neutrals remain in the ionisation source and the measurement time is initiated. The drift tube can vary in length from 5 centimetres to 3 metres or more. An electric field gradient, typically from 10-100 Vcm^{-1}, from the ionisation source to the detector causes the ions to traverse the drift tube at a constant velocity. A drift gas is introduced counter-current to the flow of ions keeping the drift-tube free of neutrals which could participate in ion-neutral clusters.

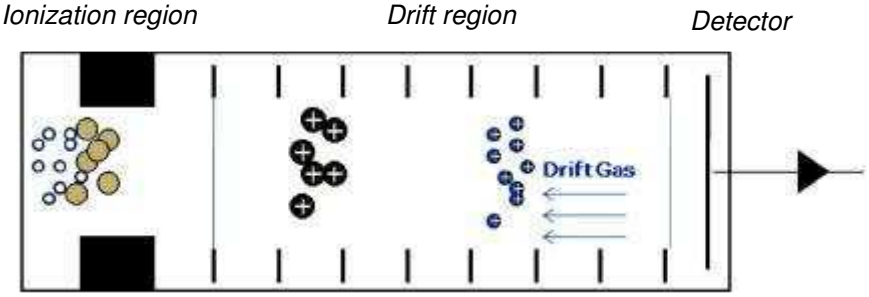

FIGURE 3. Illustration of DT-IMS, adapted from Eiceman and Karpas (2004). A voltage gradient is applied to the ions from left to right.

The total ion signal is detected and plotted with respect to time to form an ion mobility spectrum, e.g. (see FIGURE 4) for a mixture of amphetamines analysed by ESI-DT-IMS-MS (Matz and Hill, 2002). Smaller ions travel faster through the drift region and have shorter drift times, compared to higher molecular weight ions that drift slower and possess longer drift times.

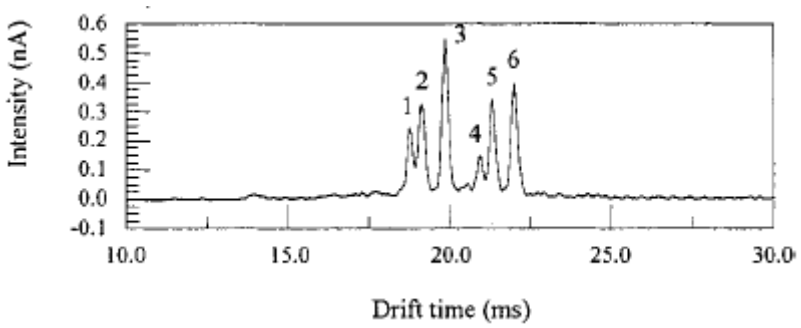

FIGURE 4. ESI-DT-IMS-MS spectrum of a mixture of 1) amphetamine, 2) methamphetamine, 3) ethylamphetamine, 4) 3,4-methyldioxyamphetamine, 5) 3,4-methylenedioxy methamphetamine and 6) 3,4-methylenedioxyethylamphetamine, adapted from Matz and Hill (2002a).

Another complementary approach to classical DT-IMS-MS was the use of the second quadrupole (Figure 5) in a triple-quadrupole mass spectrometer as an ion mobility device; while this approach was never commercialized it did open up opportunities in hyphenation of IMS and MS. In the triple quadrupole energy loss method an incident ion is transmitted to the second quadrupole of a triple quadrupole mass spectrometer where the ion will experience a drag coefficient and generate a stopping curve; from the stopping curve the ion mobility can be measured and a collision cross-section determined. Indeed, Covey and Douglas (1993) were the first to measure collision cross- sections for some biomolecules using this method and also later reviewed collision dynamics in quadrupole systems including an assessment of the internal energy of the $C_6H_5^+$ ion by measuring the increase in collision cross-section after collisional activation (Douglas, 1998) .

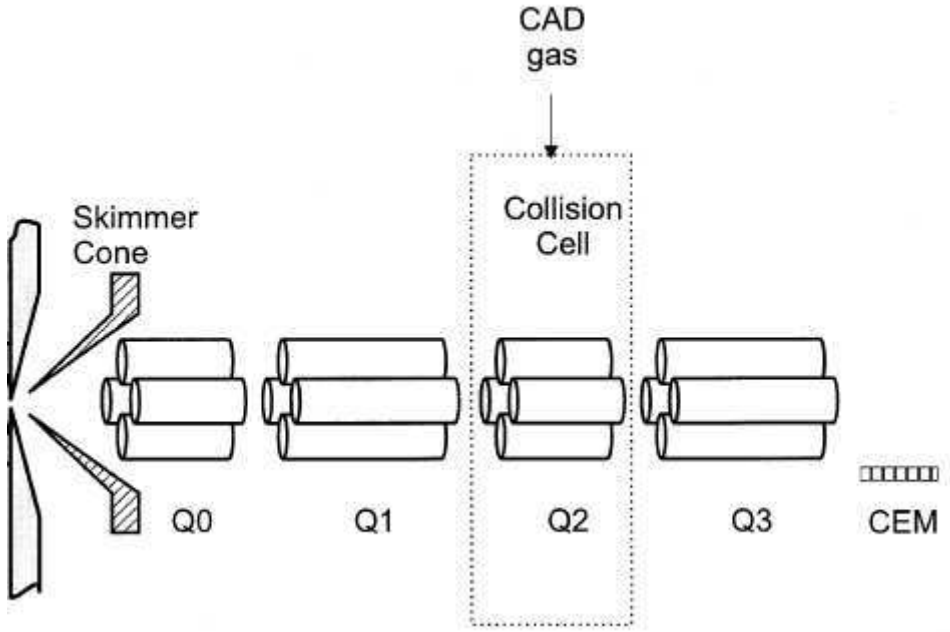

FIGURE 5. Schematic of the triple quadrupole configuration that can be used to obtain ion mobility measurements via an energy loss method, adapted from Purves et al. (2000).

This triple-quadrupole energy loss method was further developed to utilise segmented collision cell rods separated by small 1 mm gaps that enabled a radio-frequency only quadrupole drift cell to be used to reduce ion losses due to diffusion and enable mass selection before or after the drift cell, and a DC gradient that moved the ions in an axial direction (see Figure 6, Javahery & Thomson, 1997). Unfortunately this configuration was outside the typical low-field IMS range and may have resulted in field-heating of ions. This configuration was later improved to possess an increased gas pressure and lower field concentration that resulted in minimal internal excitation of the ions (Guo et al. 2004).

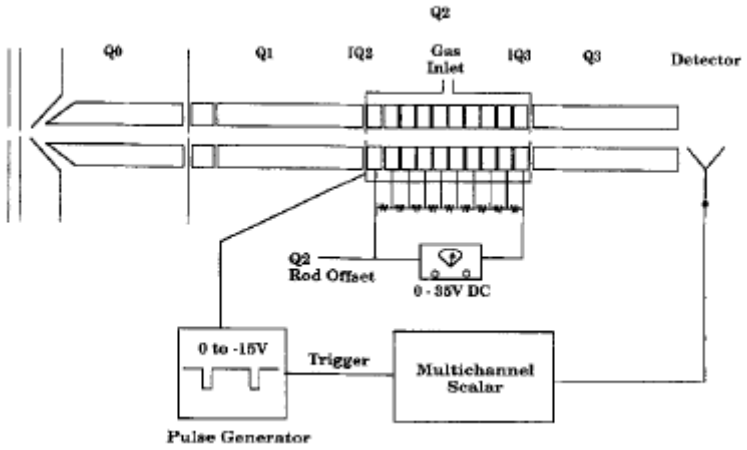

FIGURE 6. Schematic of a segmented triple quadrupole configuration that can be used to obtain ion mobility measurements, adapted from Javahery & Thomson (1997).

(ii) Differential mobility IMS (DMS) or FAIMS uses a sequence of intermediate and high field regimes where the behaviour of ions is described empirically by the Mason-Schamp equation (Mason and McDaniel, 1988) under a high-field regime, which can be expanded to an infinite series of E/N:

$$K_0(E) = K_0(1 + a(E/N)^2 + b(E/N)^4 + c(E/N)^6 + ...) \quad (5)$$

where K_0 is the reduced ion mobility, E is the field intensity and N is the buffer gas number density. However, under a typical FAIMS electric field the mobility can be approximated by using the first two factors as the importance of the sixth order and higher are insignificant (the fourth order is two orders of magnitude smaller than second order, and the second order is three to five orders of magnitude smaller than one (see Shvartsburg et al., 2004).

The basic principle of operation is that ions are introduced to a region with electrodes and a stream of gas acts as a transport medium. An asymmetric waveform is passed across the electrodes, which consists of a high potential electric field for a short time followed by a low potential electric field for a longer time; this typically fixed dispersion voltage (DV) waveform is superimposed with a variable compensation voltage (CV) to maintain a stable trajectory for the analyte ion. This process will effectively select ions and act as an ion filter, as shown in Figure 7. A cylindrical electrode configuration has usually been designated FAIMS, whereas parallel plate configurations have typically been designated as DMS.

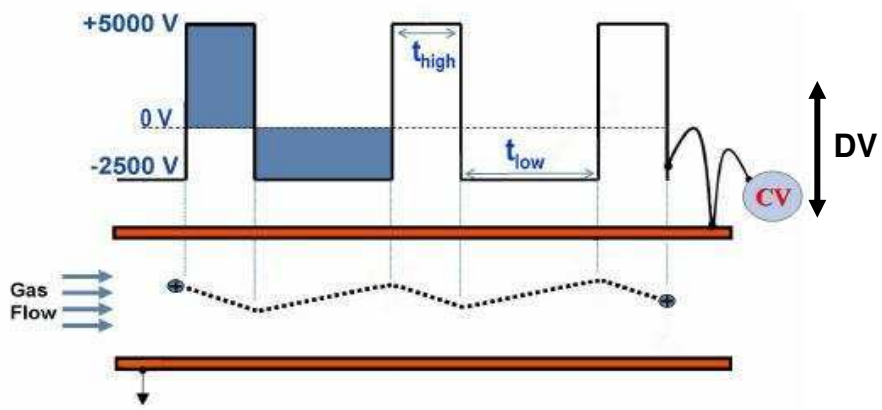

FIGURE 7. Illustration of an example of a parallel plate DMS with compensation voltage applied showing ion transmission, adapted from Thermo Fisher Scientific Inc., FAIMS Operators manual (2007).

A compensation voltage scan measurement (Figure 8) shows a typical profile attained by optimising the effect of inner and outer electrode temperatures on peak profile for morphine and its 3-β-D-glucuronide metabolite (Hatsis et al., 2007). Optimising the separation of morphine whilst maintaining sensitivity was reported to enable the metabolite interference to be effectively filtered out, and significantly improve the quantification of morphine.

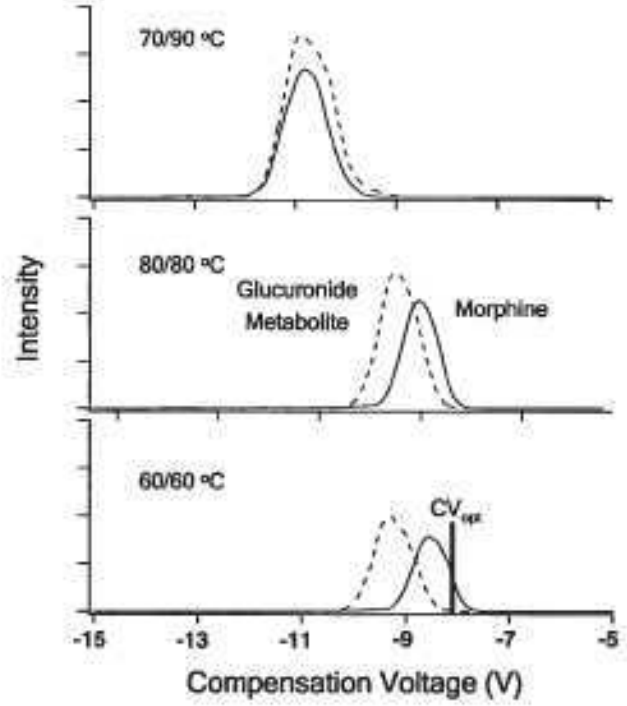

FIGURE 8. Compensation voltage scans of morphine and the glucoronide metabolite, adapted from Hatsis et al., (2007).

The use of compensation voltage optimisation to select an analyte ion can result in a clear difference in the mass spectrum observed resulting in an increased S:N ratio for the analyte and a reduction in other signals as shown in the use of ESI-FAIMS-MS with cisplatin and its hydrolysis products (Cui et al., 2003) shown in FIGURE 9.

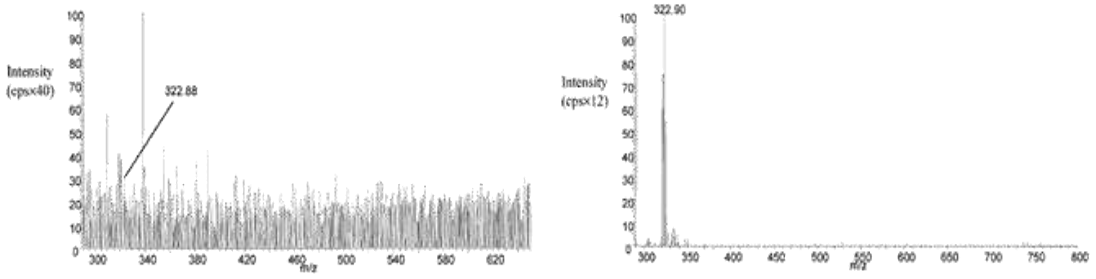

FIGURE 9. Mass spectra showing the reduction in background noise from (a) ESI-MS to (b) ESI-FAIMS-MS, adapted from Cui et al. (2003).

Currently the factors determining the separation mechanism in FAIMS or DMS and factors governing peak width as well as transmission remain relatively difficult to predict (Shvartsburg et al., 2004). The parameters influencing performance include field intensity, ion path length, gas properties (composition, temperature, pressure), shape and width of electrodes, the profile and frequency of asymmetric waveform, compensation voltage scan speed and gas flow. Champarnaud et al., (2009) studied the separation of trace level impurities by combining experimental observation with a Design of Experiment (DOE) statistical treatment that indicated important factors in the optimisation of the values of the compensation voltage, signal intensity, separation, peak asymmetry and peak width. However, a study of tetraalkylammonium ions found standard conditions were often suitable for selecting ions with an m/z value of 100-700 (Aksenov and Kapron, 2010). The simulation of ion motion in planar electrode FAIMS and cylindrical electrode FAIMS, provided insights into design, experimental variables and interpretation (Smith et al., 2009b) and some of the key molecular and instrumental parameters affecting performance were discussed by Nazarov (2006) and Levin et al. (2004).

Whilst there are several novel geometries (Prieto, 2011), there are two main forms of field asymmetrical waveform ion mobility spectrometers: 1) those with planar electrode geometry and 2) those with curved electrode geometry. Both planar geometry and the curved geometries of FAIMS and DMS evolved during the 1990s, and in the early 1990s the term differential mobility spectrometry (DMS) became generally synonymous with planar electrodes and the term FAIMS became synonymous with curved geometries, although there are multiple examples of overlapping usage of the terms DMS and FAIMS. One of the primary differences relates to the use of polar transport gas modifiers. Planar devices create homogeneous electric fields which enables the use of transport gas modifiers without resolution losses whereas curved geometries tend to create inhomogeneous fields which lead to a loss in resolution when using transport gas modifiers. However, curved geometries have been shown to provide some degree of ion focusing at atmospheric pressure resulting in higher sensitivity (Guevremont & Purves, 1999; Krylov, 1999). Planar line-of-sight analyzers enjoy the convenience of transmitting all ions when the RF voltages are turned off, so that operation without mobility separation can be achieved simply by turning off the fields. Curved geometry/non line-of-sight FAIMS require the device to be removed for operation without mobility separation. A wider analysis of the differences between alternative geometries was described by Krylov (2003).

A comprehensive review discussed the applications of FAIMS for drinking water analysis, pharmaceutical metabolite identification and separation of isomers and isobaric peaks (Kolakowski and Mester, 2007). In addition a detailed account of the fundamentals of DMS and FAIMS has been written by Shvartsburg (Shvartsburg, 2010).

(iii) Travelling wave ion mobility spectrometry (TWIMS) is a novel method whereby ions are separated according to their mobility in a series of voltage pulses in a travelling wave (T-wave) mobility cell utilising RF ion guides (Gerlich, 1993). The resolving power is relatively low; however, collision cross-sections can be derived by calibration with known standards. This ion mobility approach has been successfully interfaced to a conventional time of flight mass spectrometer and, due to the trapping gates and fast data acquisition rate of the TOF, good sensitivity is achieved. Despite attempts (Shvartsburg and Smith, 2008; Smith et al., 2009a)

the motion of ions in TWIMS is not fully understood and TWIMS calibration is typically used to calculate CCS values. The commercial technical and software support has arguably reinforced attempts to utilise IMS-MS in separation, characterization and measurement applications, for example, via the routine use of multidimensional data in Driftscope software (Williams et al., 2009a) and software to process complex data such as time-aligned parallel fragmentation (D'Agostino and Chenier, 2010).

In travelling wave ion mobility spectrometry a transient DC voltage pulse is applied in order to create an electromotive force via a series of sequentially opposite polarity RF-only rings to create a travelling wave which propels ions through the device, as shown in Figure 10. Ions with high ion mobility slip behind the wave less often (or spend more time surfing) than ions of low ion mobility thus enabling separation based on relative ion mobility.

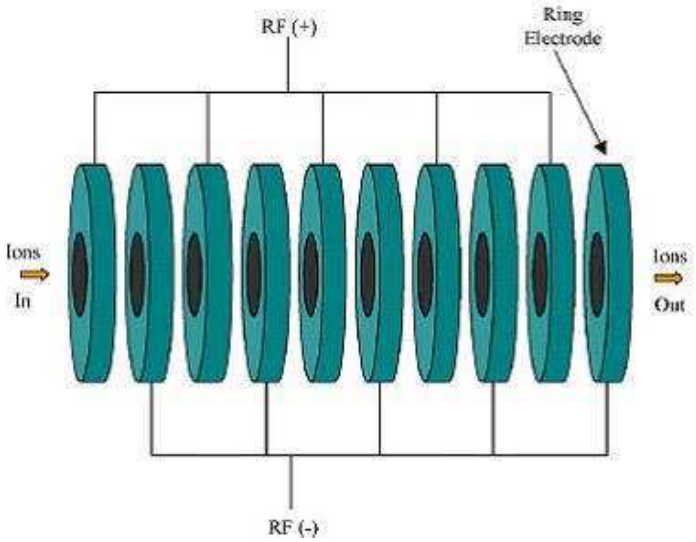

FIGURE 10. Illustration of a stacked ring ion guide used in traveling wave ion mobility spectrometry (TWIMS), adapted from Pringle et al. (2007).

Visualising data obtained using the proprietary Driftscope software enables a range of options for understanding the data including 3D visualisation, 2D plots and intensity views etc, The data can be interactively processed if desired, for example, to show data that only contains a certain component using various geometric selection tools such as lasso and square area.

(iv) The Differential Mobility Analyser (DMA) was originally developed to generate particles in order to calibrate aerosol instruments, later expanded to describe the mobility of non-diffusing particles by Knutson and Whitby (1975) and recently to describe the mobility of diffusing particles by Stolzenberg & McMurray (2008). The DMA consists of a combination of electric field mobility in addition to a fast gas stream, only ions with a well defined electrical mobility are transmitted into an outlet slit leading to the mass spectrometer inlet (see Figure 11). The DMA vacuum regime means that the measured ions do not experience a vacuum interface or ion guide so may be less prone to structural modifications (Hogan et al., 2011) and, as the separation technique is a space-dispersion rather than a time-dispersion technique, the ions can be continuously transmitted to a mass spectrometer.

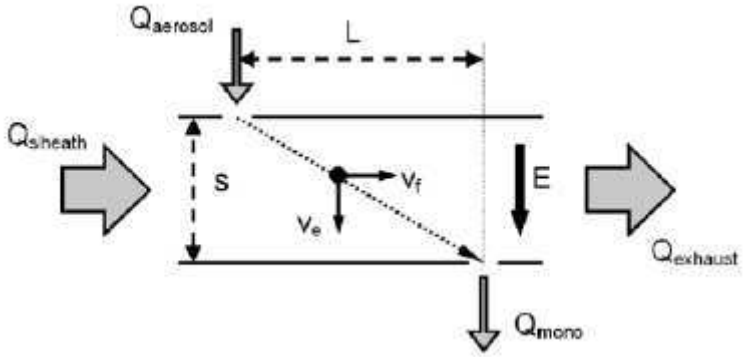

FIGURE 11. Schematic of the operation of a differential mobility analyzer. Ion are injected at the top left and move downwards and to the right, over a distance S, under the influence of an electric field E, adapted from de la Mora et al., (2006)

The DMA technique may be considered a hybrid of DT-IMS and DMS as the separation process is based on the low electric field mobility like DT-IMS, however the sampling is continuous as in DMS. DMA-MS has been most widely explored for large molecules; however, discussion on multiple charged polyethylene glycol ions (Ude et al. 2004) illuminated structures from approximately 300 Da to 3000 Da describing configurations for long straight chain molecules. One of the advantages of DMA is that it can, theoretically, be easily added to existing mass spectrometry stages without complex interfaces due to operation at atmospheric pressure (Rus et al., 2010). A DMA was coupled to an existing Sciex QStar MS (Concord, ON, Canada) enabling separation of L-alanine and an isomer, sarcosine, (Martínez-Lozano P et al., 2010) which are proposed to be small molecule biomarkers from urine in the progress of prostate cancer.

IMS covers a range of different techniques and unfortunately some gross simplifications have resulted in terminology that may be confusing.

1. DTIMS is also known as Classical IMS, Conventional IMS, Standard IMS, Drift-Tube IMS, Time of flight IMS, Traditional IMS, Plasma Chromatography and Ion Chromatography.
2. DMS includes High Field Asymmetric Waveform IMS (FAIMS), Field Ion Spectrometry and Ion mobility Spectroscopy and is commercialised in the Ionalytics Selectra, Thermo FAIMS, Owlstone Nanotechnologies and AB Sciex Selectra systems.
3. Travelling wave ion mobility spectrometry (TWIMS) is commercialised in the Waters Synapt systems.
4. Differential Mobility Analysers (DMA) have been developed by several groups at Yale (USA), CIEMAT (Madrid) and RAMEM (Madrid).

Comparison of key benefits and challenges of IMS-MS methods

There is currently a wealth of IMS-MS systems available both commercially and being used and developed in academic institutions.

DT-IMS-MS has been most widely used in academic institutions and provided some of the highest resolving powers. An advantage of DT-IMS-MS is that the ion mobility can be determined experimentally and collision cross section determined without requiring calibration. A key challenge is that the pulsed analysis leads to an inherent loss of duty cycle and hence reduction in sensitivity.

An advantage of both DMS-MS and FAIMS-MS is that it operates as a continuous device when the compensation voltage is selected so does not have the 'lossy' sampling issues of DT-IMS and TWIMS. The separation appears to be orthogonal to m/z and sometimes size so that separations may be uniquely tuned to select a chosen analyte and thus be used as a powerful separation technique. A key challenge is that it has proven difficult to definitively assign structural properties and changes to DMS measurements as several factors appear to contribute to the clustering/declustering mechanism and analyte drift times thus it appears to be best utilized as a separation device.

An advantage of TWIMS-MS is that it is commercially supported and that the ion mobility can be determined experimentally and collision cross-section determined with suitable calibration. Whilst the

resolution obtained in TWIMS is typically lower than dedicated DT-IMS-MS and some FAIMS/DMS the software to interpret and process the complex data is well supported.

Advantages of DMA-MS include operation in the low electric field regime that typically means less structural distortions and determination of collision cross-section, a continuous sampling rate that should mitigate sensitivity losses (with reported transmission efficiencies of up to 50% (Martínez-Lozano et al., 2011)) and the theoretical ability to add the device as a front-end to many existing mass spectrometer systems. However DMA-MS has not been fully commercialized yet or utilized for the multitude of "small molecule" applications explored in DT-IMS-MS, FAIMS-MS, DMS-MS and TWIMS-MS though it shows significant promise.

C. Understanding IMS-MS resolving power and selectivity

IMS can separate analytes based on their ion mobility including closely related species such as isomers (Williams et al., 2010), isobars and isotopomers (Shvartsburg et al., 2010a). The key parameters affecting a useful separation are 1) the resolving power and 2) the selectivity.

Resolution and peak capacity in IMS

The combination of ion mobility and mass spectrometry in IMS-MS offers a technique that is able to distinguish components based on their size to charge ratio (Ω/*z* for IMS) and mass to charge ratio (*m/z* for MS), thereby enabling orthogonal specificity. Even with expensive high-resolution mass spectrometer systems affording $m/\Delta m_{50\%}$ resolution of over 400,000 it is still analytically challenging to differentiate between isomeric components and often complex MS^n experiments are required to achieve selectivity for unambiguous assignment. Ion mobility can provide extra resolving power, however IMS used alone is currently unable to unambiguously identify an unknown molecular component without *a priori* knowledge of the measured drift time.

It is possible to measure the resolving power of ion mobility using a single quotient definition (Siems et al., 1994):

$$R = dt / wh \qquad (6)$$

where *R* is the resolving power of the IMS, *dt* is the drift time of the ion of interest and *wh* is the full peak width measured at half height. Resolving power is a measure of the efficiency of an instrument to separate two peaks. The Waters Synapt G2 IMS system has been developed to encompass a resolving power of up to 40; FAIMS resolving powers of up to 100 (Shvartsburg et al., 2010b) have been achieved, and several reports of resolving powers of up to 225 with DT-IMS have been reported (Koeniger et al., 2006; Shelimov et al., 1997; Kemper et al., 2009). Developments including higher pressure trapping and focussing (Clowers et al., 2008), overtone ion-mobility (Valentine et al., 2009) and circular instruments (Bohrer et al., 2008) are expected to exceed these current limitations.

The number of theoretical plates is a mathematical concept, relevant in any chromatographic technique, which is often used to describe column efficiency and is an indirect measure of the peak width for a peak at a specific retention time:

$$N = 5.545\left(\frac{t_R}{W_h}\right)^2 \qquad (7)$$

where N = number of plates, t_R = retention time and W_h = peak width at half height (in units of time). The number of theoretical plates is typically used to compare chromatographic systems and the data in Table 2 compares various types of IMS with typical traditional chromatographic techniques.

TABLE 2. A comparison of required resolving power in theoretical plates for various types of IMS compared to typical chromatographic conditions.

Approximate number of theoretical plates	Required resolving power of equivalent	Comparative chromatography conditions

	IMS	
20000	60	High performance liquid chromatography (HPLC)
80000	120	Ultra high performance liquid chromatography (UHPLC)
125000	150	Gas chromatography (GC)
222000	*200*	*High resolution IMS (Asbury & Hill, 2000a)*
887000	400	Capillary electrophoresis (CE)

Therefore, a current high-resolution IMS resolving power of 200 is roughly equivalent to a chromatographic efficiency of >200,000 theoretical plates.

Peak capacity of IMS-MS

Complex samples require high efficiency to achieve separation and, even in early stage drug discovery, having a high efficiency affords a good opportunity to separate degradants and process impurities away from the desired product. Peak capacity is defined as the maximum number of peaks that can fit in any two-dimensional method (Ruotolo et al., 2002a). A two-dimensional method will have a high peak capacity if the resolution of each dimension is high and the difference in their separation mechanism (orthogonality) is high. The peak capacity will also be defined by the complexity of the sample and the properties of the analytes in the sample. For example, complex biological samples with a range of retention times will provide larger peak capacities for a technique than that of the analysis of a mixture of analytes of a specific class. Peak capacity is therefore a better, but highly molecule dependent, indicator of the separation power compared to measuring resolution alone.

In an ideal situation the peak capacity of a two-dimensional method is the product of the first and second dimensions (Li et al., 2009), but corrections can be made for cases where the two dimensions are not 100% orthogonal. Whilst the separation based on their size to charge ratio (*Ω/z* for IMS) and mass to charge (*m/z* for MS) ratio is, to some extent, orthogonal there is a well-known correlation between mobility (∝ size) and mass (Griffin et al., 1973), as illustrated in Figure 12.

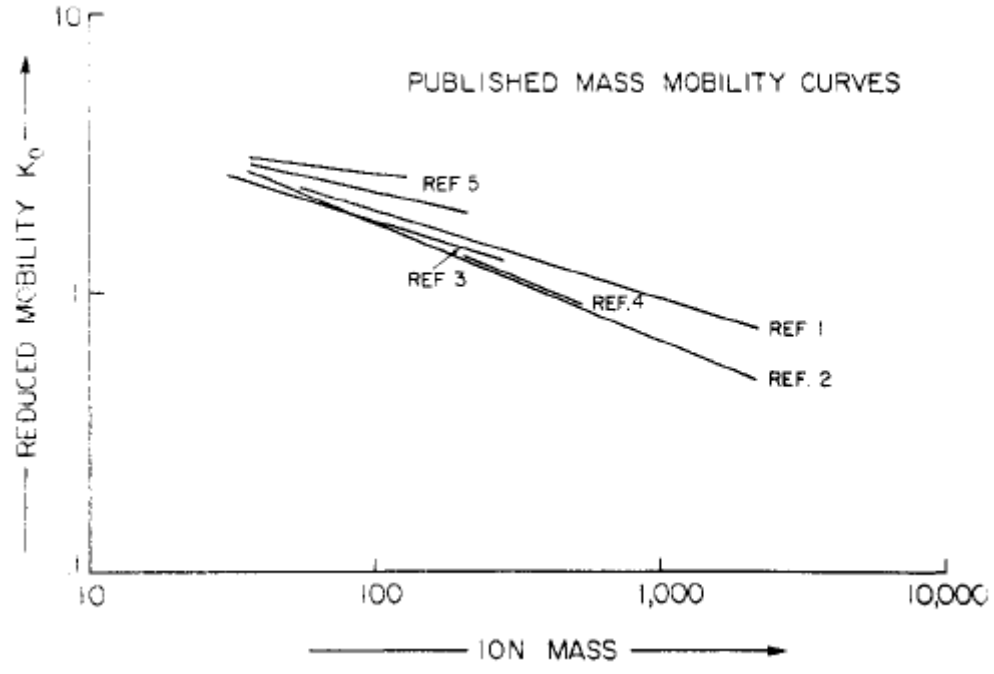

FIGURE 12. Published mass mobility curves showing correlation between reduced mobility and mass within classes, but poor correlation in heterogeneous sets, adapted from Griffin et al. (1973).

Therefore the corrected peak capacity, P_c, in IMS-MS can theoretically be estimated (Dwivedi et al., 2010) using the relationship:

$$P_c = R_{IMS} \times R_{MS} \times \text{fraction of orthogonality} \quad (8)$$

where R_{IMS} is the average resolving power of the ion mobility spectrometer, and R_{MS} is the average resolution of the mass spectrometer.

An example of increased peak capacity in IMS-MS was observed in a study of various classes of metabolites in blood (Dwivedi et al., 2010) including amino acids, organic acids, fatty acids, purines etc) using a DT-IMS-MS system. In the mass range of 23 – 830 m/z, the drift time spread of ~14.3 ms results in ~28% of the total 2D space, or an average deviation in drift time of ±14% along the theoretical trend. With an average IMS resolving power of 90, average MS resolution of 1500, and ±14% orthogonality, the estimated peak capacity, P_c, for the instrument is 90 x 1500 x 14% = 18,900. The relatively low MS resolution of 1500 (peak width is 0.27 Da at an average mass value of 404 m/z) in this study (Dwivedi et al., 2010) resulted in an estimated peak capacity of MS alone of 2989. A six fold increase in the peak capacity was therefore observed (~19,000) in IMS-MS compared to MS alone (~3000).
Reverse phase chromatographic columns are routinely used to separate small molecules and the peak capacity for gradient elution high performance liquid chromatography was found to be typically up to 300 (Guo et al., 2009), and up to 400 (Wren, 2005) for gradient elution ultra-performance liquid chromatography. Comparing the peak capacity for different types of IMS with typical traditional chromatography peak capacities (Table 3) shows that the extra dimension of IMS is potentially a powerful separation tool.

TABLE 3. Approximate separation peak capacity for various analytical separation methods*.

Technique	Approximate peak capacity
FAIMS	*8.9 -44 (Canterbury et al., 2008)(Schneider et al., 2010b)*
DT-IMS	*90 (Dwivedi et al., 2010)*
HPLC	300 (Guo et al., 2009)
UHPLC	400 (Wren, 2005)
MS	3000 (Dwivedi et al., 2010)
IMS-MS	*19000 (Dwivedi et al., 2010)*
LC-MS	900000
LC-IMS-MS	*11340000 (Dwivedi et al., 2010)*

*Ion mobility and hyphenated techniques are italicized

It is conceivable that LC-IMS-MS may become a standard addition or replacement for LC-MS systems due to the ease of configuration and the increase in separating power. Indeed many proteomic applications are increasingly using LC-IMS-MS to separate complex peptide mixtures, leading to unprecedented extensive proteome maps (Liu et al., 2007b; Taraszka et al., 2005). LC-IMS-MS often does not require careful configuration, demanding sampling rates and does not appear to suffer from robustness issues compared to many two-dimensional techniques such as LCxLC, GCxGC etc.

Modifying selectivity in IMS

The selectivity of ion mobility can be modified by increasing the electric field in DT-IMS (Wu et al., 1998), the use of covalent shift reagents (Fenn and McLean, 2008) to derivatise or non-covalent shift reagents (Clowers and Hill, 2006; Howdle et al., 2009) to form complexes with analytes and effect a selective shift in ion mobility relative to coincident analytes, using drift gas modifiers (Fernández-Maestre et al., 2010a) sometimes called clustering agents in DMS-MS (Schneider et al., 2010b)), by altering the composition of the drift gas (Matz et al., 2002) and by the use of different reagent gases in GC-IMS-MS (Eiceman et al., 1995). Currently there does not appear to be a consensus on useful and well characterised selectivity modifiers so method development is presently not fully predictable; however some of these changes are trivial and can be considered analogous to changing the stationary or mobile phases in liquid chromatography.

The use of covalent shift reagents (Fenn and McLean, 2008), as shown in Figure 13 , effectively derivatises molecules, potentially creating lower density analogues of the precursor species with a marked increase in the collision cross-section relative to a smaller increase in mass. This is clearly

illustrated by deviations to larger cross sections compared to the general trend in mass-mobility correlation for carbohydrates. Compared to the underivatised species it was reported that covalent derivatisation afforded three distinct advantages: (i) tuneability was increased for isobaric species difficult to identify and/or resolve by mass spectrometry alone, (ii) an enhanced sensitivity of 2x more signal intensity was observed and (iii) the derivatised species could be used as tags or fragment labels in CID and as IR active species in IRMPD studies.

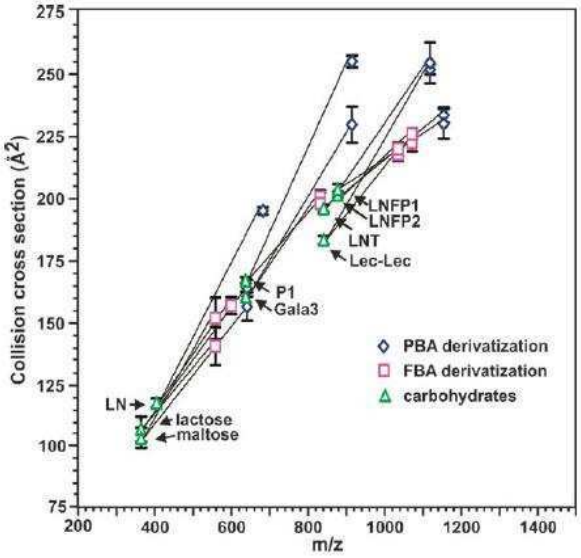

FIGURE 13. Effect of derivatisation of carbohydrate species with boronic acid on CCS, adapted from Fenn and McLean (2008).

For small molecules the effect of the dipole interaction is typically far more significant than for large molecules (>500 Da) so that using drift gas modifiers or mixtures can be a powerful method to alter selectivity (elution order of analytes). Indeed for small molecules such as amino acids the polarisabiity has been found to be a critical factor affecting separation of analytes, whereas in large molecules the collision cross section term dominates (Steiner et al., 2006). Thus for small molecules exploiting polarizability to probe structural details and maximize separation has immense future potential.

An example of the potential of exploiting polarizability to separate analytes is given by the different slopes of calculated ion radii for iodoaniline and chloroaniline with different drift gases, helium (0.205 x 10^{-24} cm^3), argon (1.641 x 10^{-24} cm^3) and carbon dioxide (2.911 x 10^{-24} cm^3), indicating that it should be possible to separate any analytes with different slopes (Figure 14) by choosing an appropriate drift gas composition.

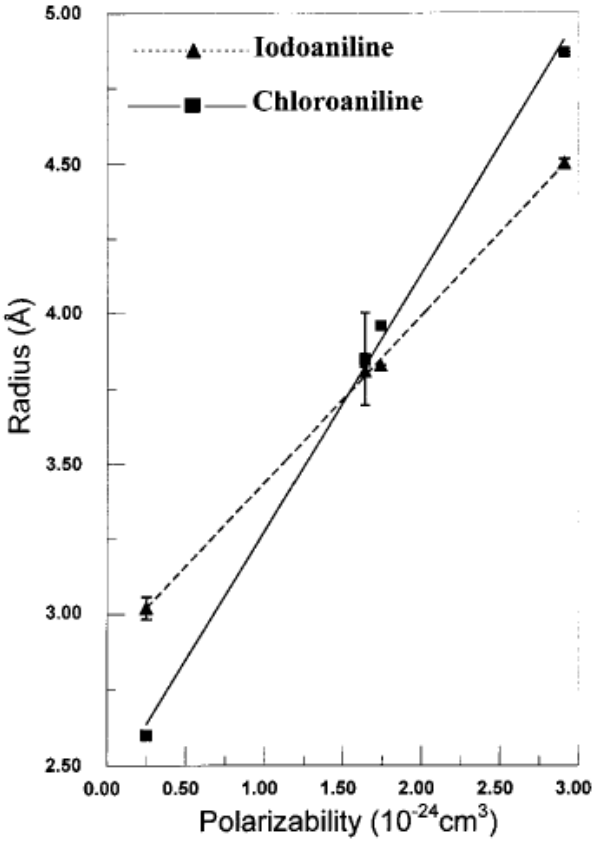

FIGURE 14. Calculated ion radii as a function of drift gas polarizability, from Asbury & Hill, 2000c.

The use of vapour modifiers added to the drift gas in planar DMS-MS has been widely explored (e.g. Levin et al., 2007 and Eiceman et al. 2004) , although the full mechanism of the interactions has not been elucidated enough to enable predictable separations in mixtures. Levin et al. (2004) systematically examined the effect of various polar clustering agents and postulated strong effects due to hydrogen-bonding potential, electrostatic attraction, steric repulsion and energetically feasible conformations. A series ofpublications exploring the cluster/declustering (Krylov et al. 2002, Krylov et al. 2009, Schneider et al. 2010a, Schneider et al. 2010c, Coy et al. 2010) further explored the possibility of predicting analyte shifts in response to changes in drift gas modification and provide a powerful route to optimising separations.

The 'cluster/declustering effect' that addition of vapour modifier induces appears to have dramatic effects on the peak capacity in a planar electrode configuration (Schneider et al., 2010b), improving the peak capacity for a 70 component mixture from 13 in pure nitrogen to 44 in 2-propanol doped nitrogen (see FIGURE 15), although this had the disadvantage that 10/70 components were depleted in intensity by 20-fold or more due to them having a lower proton affinity than the dopant.

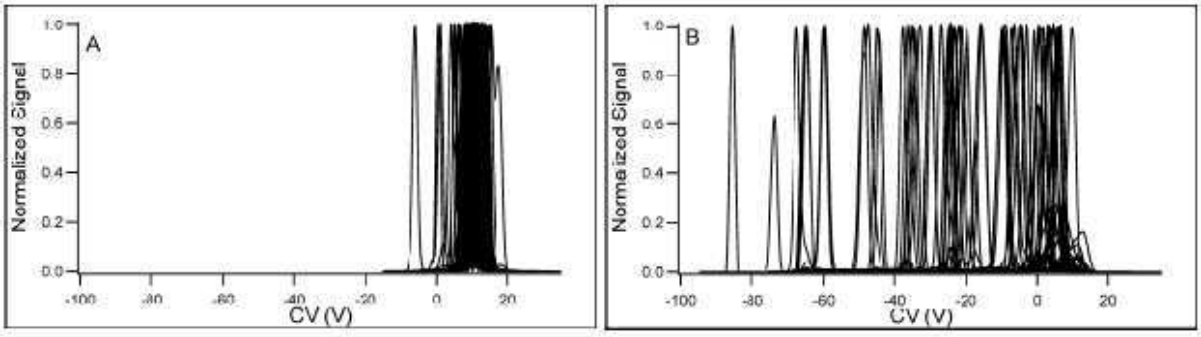

FIGURE 15. Separation of a 70-compound mixture with (A) nitrogen transport gas and (B) nitrogen with 1.5% 2-propanol in parallel plate FAIMS configuration, adapted from Schneider et al., (2010b).

Changes to the temperature, composition (Beegle et al., 2001) and pressure of a single drift gas is commonly used to change selectivity and IMS gasses including nitrogen, air, helium, carbon dioxide and sulphur hexafluoride have been evaluated. The use of binary gas mixtures (Howdle et al., 2010), shown in Figure 16, results in excellent selectivity enhancements over single gas composition IMS separations and demonstrates that this selectivity is tunable by altering the binary gas composition.

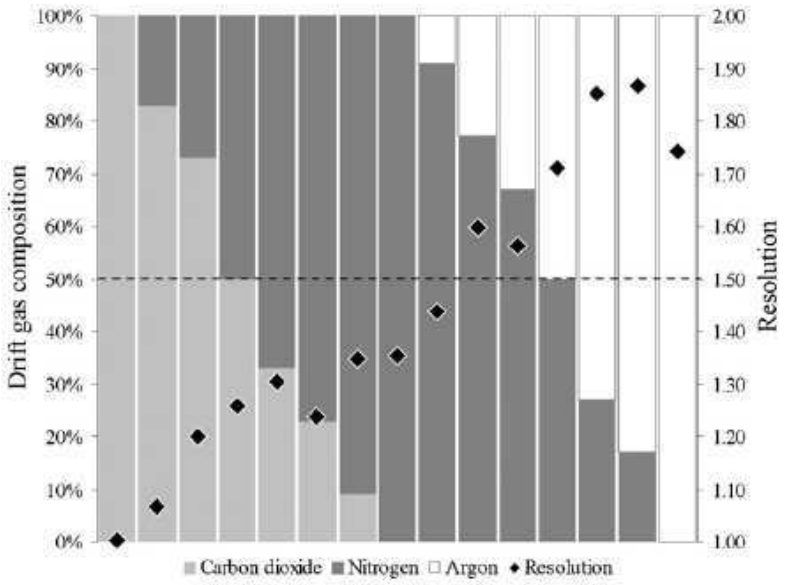

FIGURE 16. Effect of drift gas composition on the ion mobility resolution of the drugs rosiglitazone and lamotrigine $[M+H]^+$ ions in binary drift gas mixtures in TWIMS. The composition of the binary drift gas mixtures are represented by shaded bars indicating the percentage of each gas in the mixture (left hand axis). Resolving powers greater than 1.5 indicate full separation of components and this threshold is indicated by the dashed line at a resolution of 1.5. The resolution of lamotrigine and rosiglitazone is indicated by the right hand axis. Adapted from Howdle et al., (2010).

IV. APPLICATIONS OF IMS AND IMS-MS SEPARATIONS IN SMALL MOLECULE ANALYSIS

IMS has been investigated for the analysis of a wide range of small molecule applications including active pharmaceutical ingredients (Budimir et al., 2007; Karimi and Alizadeh, 2009; O'Donnell et al., 2008; Wang et al., 2007) veterinary drugs (Jafari et al., 2007), metabolites (Alonso et al., 2008), pesticides (Jafari, 2006; Keller et al., 2006; Tuovinen et al., 2000), prescription and illicit drugs (Dussy et al., 2008; Lawrence, 1986), combinatorial libraries (Collins and Lee, 2001), autonomous health diagnostics (Zhao et al., 2010) and immunoassay detection (Pris et al., 2009; Snyder et al., 1996). Here we outline some highlights of small molecule analysis using IMS-MS systems.

A. Low abundance metabolite and small molecule identification using IMS-MS

A novel use of LC-IMS-MS was demonstrated for a $5HT_3$ antagonist, ondansetron, and its aromatic hydroxyl isomeric metabolites (Dear et al., 2010) that are typically generated *in vivo* and *in vitro*. Using conventional UHPLC-MS-MS the unambiguous characterisation of the hydroxyl metabolites would not be possible as they can produce identical MS/MS spectra. Using UHPLC-MS in a biological matrix system ondansetron and metabolites display different retention times but could not be assigned without using purified standards as a reference. Using an IMS separation, shown in Figure 17, and *in silico* methods the components were identified based on their ion mobility. For these components a low number of rotatable bonds are present so the computational method is rapid, interpretation of complex NMR spectra is not required and isolation or synthesis is unnecessary to create primary standards. In this case the identity of metabolites with smaller than 1 $Å^2$ difference between their CCS was distinguished using a combination of Waters Synapt TWIMS by comparison with CCS values obtained using computational methods.

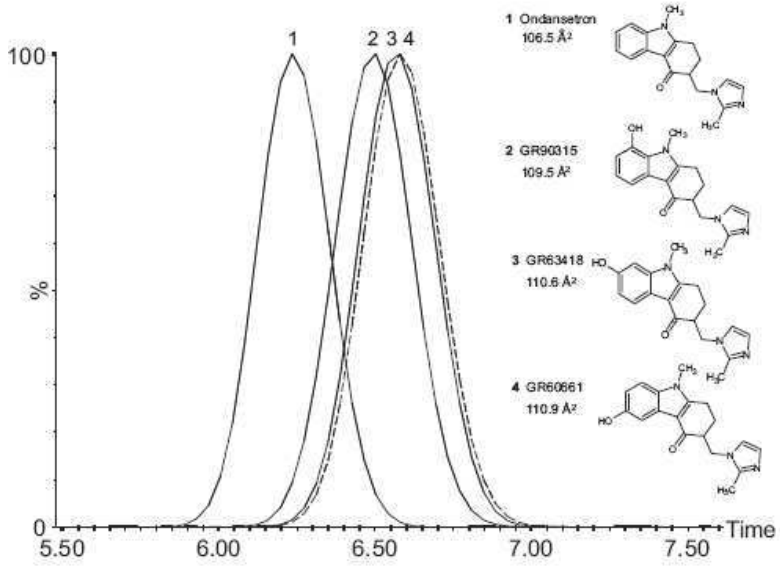

FIGURE 17. TWIMS ion mobility arrival time distributions for ondansetron and the 6-, 7- and 8-hydroxyl metabolites, adapted from Dear et al., (2010).

The subsequent use of product ion mobility as a tool for assignment of positional isomers (Cuyckens F et al., 2011) was also demonstrated for both model compounds and a real-case example, emphasizing the possibilities of structural determination by both parent ion and product ion mobility where mass spectra alone appear indistinguishable and cannot be used to confidently assign a candidate structure. For example two different product ion mobilities for 11 *ortho*, *meta* and *para* substituted hydroxyl metabolites with a phenylethylamine substructure were sufficient to assign their structures.

B. Rapid, portable and sensitive analysis using miniaturisation of IMS and IMS-MS

One of the advantages of FAIMS is that it does not require complicated vacuum equipment or large analyser tubes, thus it may be easily hyphenated to a portable mass spectrometer system (Manard et al., 2010). Microfabricated FAIMS chips can increase the speed of separation by 100-10,000 times, filtering ions on the microsecond timescale enabling rapid monitoring of species at low level concentrations (Shvartsburg et al., 2009a). Whilst the current microfabricated FAIMS units, example shown in Figure 18, are more suited to distinguish compound classes than individual species the multichannel FAIMS electrodes enables integration with an air sampler, ionisation source and detector for applications such as gas analysis, chemical monitoring and autonomous health diagnostics (Zhao et al., 2010).

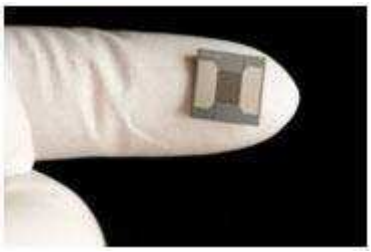

FIGURE 18. Illustration of the size of microfabricated FAIMS chip, courtesy of Owlstone Nanotechnologies and Pacific Northwest National Laboratory.

C. Increased selectivity in ambient and surface analysis mass spectrometry using IMS-MS

The direct and rapid analysis of substances using ambient ionisation mass spectrometry sources allows mass spectrometry data to be obtained with little or no sample preparation required for a variety of surfaces and matrices from tissue samples to intact tablet or liquid formulations. Application areas have included quantitative and qualitative measurements in pharmaceutical analysis, forensics, bioanalysis, *in vivo* imaging, proteomics etc. Whilst MALDI has been widely adopted in biological applications, for the analyses of biomolecules, there is currently a great deal of interest in ambient mass spectrometry approaches and there are now at least thirty methods documented (Weston, 2010).

The introduction of an additional IMS stage adds a further separation step to ambient mass spectrometry analysis without the need for rigorous sample preparation. Indeed for most surface analysis mass spectrometry methods the fact that the surface is sampled and ions are generated in a single step means that the only viable method of separation and selectivity before the mass detector is to use a gas-phase separation method such as IMS. This extra selectivity maybe particularly useful in imaging applications. In the case of the example of whole-body imaging of rats, the rats were dosed with 6 mg/kg *iv* with the anticancer drug vinblastine and the removal of interfering isobaric ions from endogenous lipids helps increase confidence in the MALDI imaging data (Jackson et al., 2007) by removing 'false positives' which, by mass spectrometry imaging alone, could be interpreted as containing a high concentration of the active drug, as shown in Figure 19. The extra dimension of separation could also prove useful in removing any matrix-related isobaric ions. The datasets from the Driftscope imaging platform were transferred to Biomap 3.7.5.5 for visualization enabling facile interpretation.

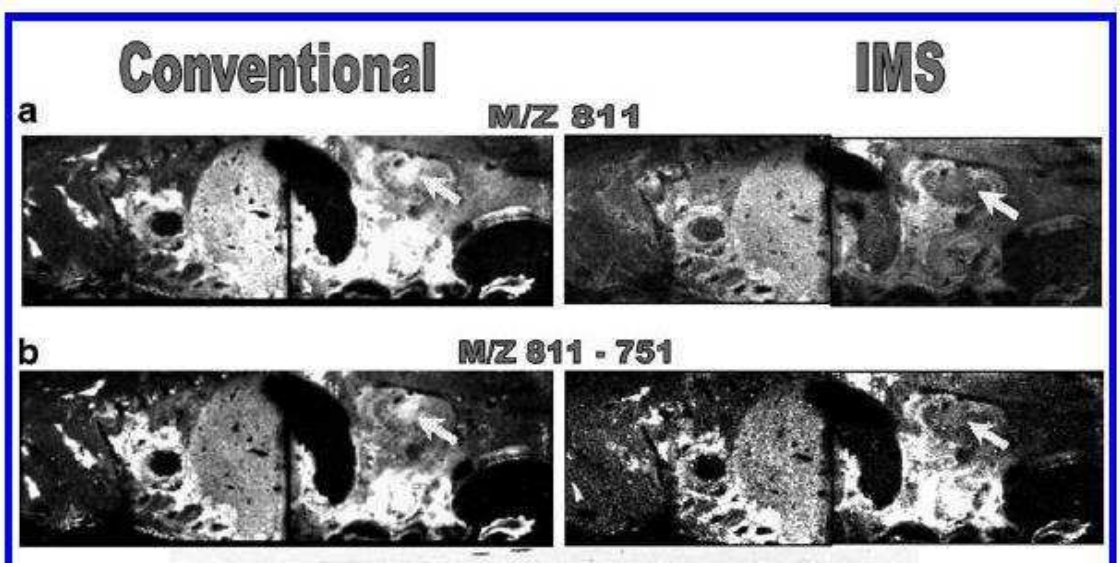

FIGURE 19 . MALDI-IMS-MS image showing distribution of ions in whole-body sections and the arrow points to the area where specificity increased with application of IMS, adapted from Jackson et al., (2007).

D. Chiral analysis using IMS-MS

A chiral modifier at 10 ppm of (S)-(+)-2-butanol was added to the buffer gas and enantiomers of a β-blocker, atenolol, were separated (Dwivedi et al., 2006), as shown in Figure 20. It is proposed that selective interactions occur in the gas-phase between the enantiomer ion and the chiral modifier, to temporarily form a diastereomeric pair, so that the mobilities of the enantiomers are altered and can be separated in time. Chiral ESI-DT-IMS-MS is now commercialised viathe Excellims Corp IMS-quadrupole-MS system. A smaller, portable chiral IMS detector is now being developed by Excellims Corp for fast, on-site analysis including pesticide residues and environmental samples (Anon). The advantages of chiral IMS-MS compared to competing analytical techniques such as chiral SFC and chiral HPLC include rapid method development and high sensitivity, enabling rapid determination of enantiomeric excess (e.e.) for use in QA/QC environments or in broader applications including biomarker and metabolite identification.

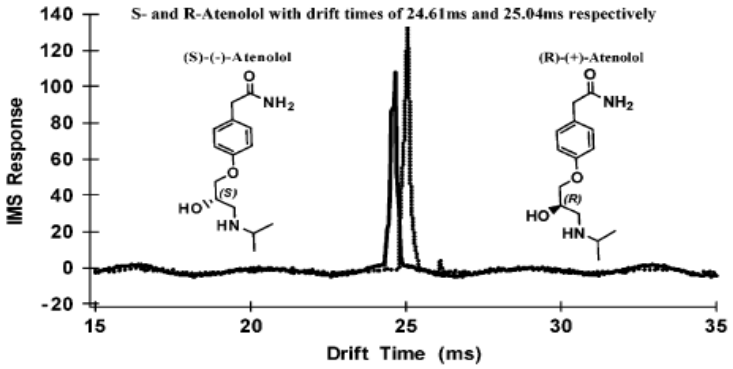

FIGURE 20. DT-IMS-MS separation of atenolol enantiomers showing the superimposed spectrum of the R and S enantiomers (similar results obtained using racemic mixture, not shown). Adapted from Dwivedi et al., (2006).

Chiral resolution using FAIMS-MS has also been reported for 6 pairs of amino acid enantiomers separated as metal-bound complexes of divalent metal ion with an L-form amino acid (Mie et al.,

2007), shown in Figure 21. The method employed a range of additional divalent metal cations and reference amino acids. Screening with different metal cations and reference compounds compares favourably with chiral HPLC and SFC screening times and can be automated using automated sample preparation platforms.

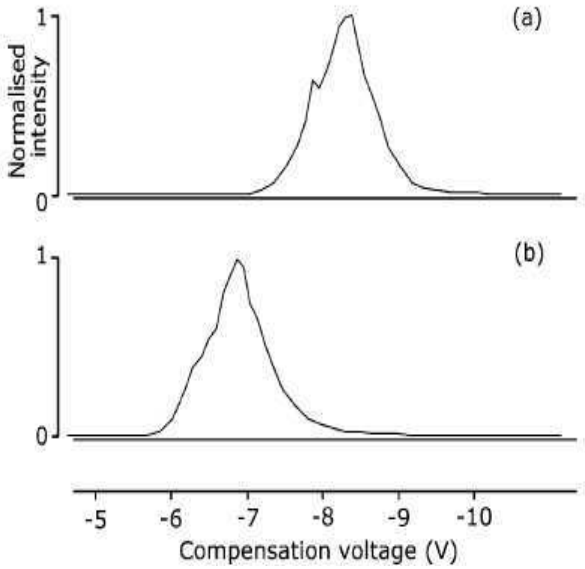

FIGURE 21. Separation of D/L-valine as $[Cu^{2+}(l\text{-}Trp)_2(D/L\text{-}Val)\text{-}H]^+$. (a) D-Val; (b) L-Val. Adapted from Mie et al., (2007) .

An example of epimer separation where the diastereomers differ by only one chiral carbon, was achieved for betamethasone and dexamethasone (Campuzano et al., 2011). The separation of the two epimers correlated well with differences observed in the calculated B3LYP/6-31G++(d,p) electrostatic potential surface. Whilst baseline separation is achievable by HPLC (Arthur et al., 2004) the mass spectra of these compounds is very similar so the rapid separation and correlation with molecular modeling quickly identify this pair of compounds.

E. Resolution of isobars and isomers in complex mixtures using IMS-MS

Over 1100 metabolites were detected from methanolic extracts of 50 ul of blood samples including separation of over 300 isobaric/isomeric components, achieved without pre-concentration (Dwivedi et al., 2010), shown in Figure 22. The peak capacity compared tomass spectrometric analysis alone was increased by ~6 times and a broad range of metabolites were detected including lipids, carbohydrates, isoprenoids and estrogens. Interpretation of the data is further enabled by examining characteristic mobility-mass correlation data to identify similar classes of metabolites. In addition a reduction in the background noise due to selective ion filtering enabled detection and identification of low abundance components.

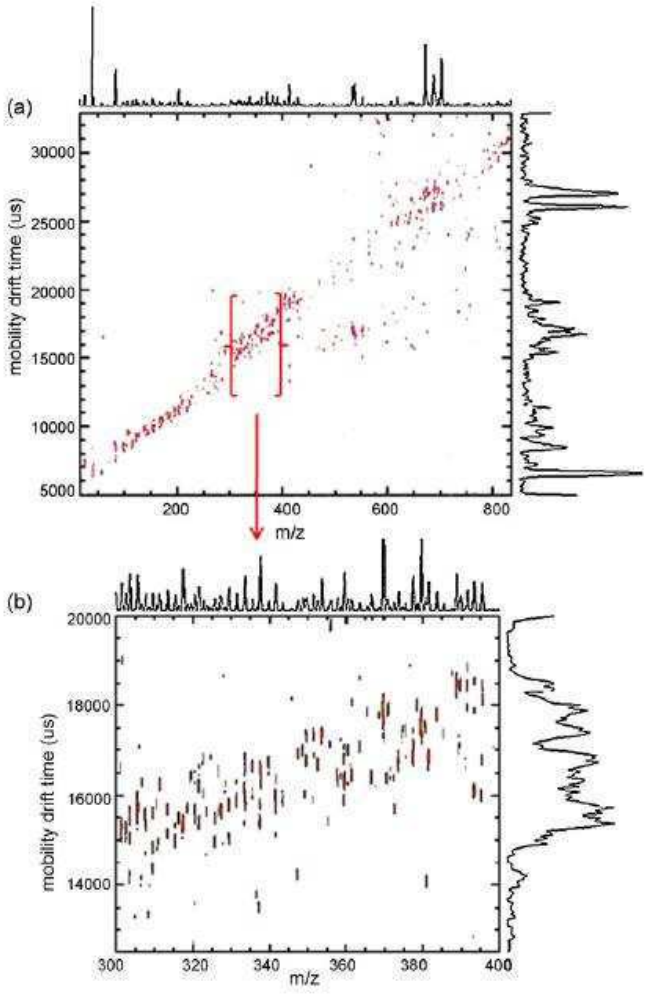

FIGURE 22. (a) Two-dimensional spectra of metabolic features measured in methanolic extract of human blood (b) a zoomed in region of the DT-IMS-MS spectrum illustrating peaks detected at the same nominal mass with different mobilities showing separation of isomers and isobars, adapted from Dwivedi et al., (2010).

F. Real-time reaction monitoring and process monitoring using IMS-MS

Reaction-monitoring in real-time has the potential to enable understanding of when reactions can be terminated at a suitable, rather than arbitrary, endpoint. By monitoring a process regularly throughout the reaction time knowledge may also be accrued of the reaction, intermediates and product formation that could not be understood by irregular, sparse sampling alone and enable optimization of experimental parameters via chemometrics. The products formed by deprotonation of 7-fluoro-6-hydroxy-2-methylindole with sodium hydroxide were monitored by TWIMS-MS (Harry et al., 2011) and showed complementary and extra information from TWIMS-MS compared to MS alone with shape selectivity information obtained by sampling every several minutes over a timescale of several hours (Figure 23).

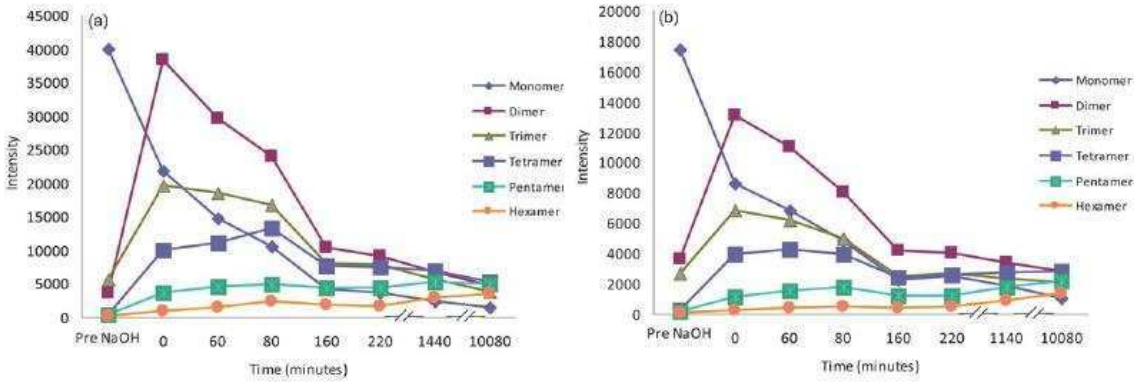

FIGURE 23. MS and TWIMS-MS analysis of the reaction of 7-fluoro-6-hydroxy-2-methylindole following the addition of aqueous sodium hydroxide. Signal response versus time in minutes for m/z 166 (monomer, I), m/z 311 (*O*-linked dimer, II), m/z 456 (*O*-linked trimer), m/z 601 (*O*-linked tetramer), m/z 746 (*O*-linked pentamer) and m/z 891 (*O*-linked hexamer) using (a) MS and (b) IM-MS. Adapted from Harry et al., (2011).

G. Rapid resolution of carbohydrate isomers using IMS-MS

Carbohydrate isomers including oligosaccharides are involved in numerous biological processes, such as cell-cell recognition and the development of embryos, but one of the main functions of carbohydrates is as oxidisable substrates in catabolism. However, to fully understand their different roles and functions we need to understand both the linkage type and anomeric configuration whilst dealing with the challenge that, for example, in a mixture of 16 D and L-aldohexoses and 8 D and L-aldoses the total number of isomers with the same mass will be 96. The use of mass spectrometry as a tool is hindered by the similarity between fragmentation data obtained for different isomers; however purification and determination of purity by NMR requires interpretation time and larger amounts of material. Separation of the metal ion adducts of anomeric methyl glycoside isomers (MeMan, MeGal and MeGlc) and isomeric forms of reducing sugars (Dwivedi et al., 2007), branch isomers, and very closely related isomers varying at a single stereochemical position (Zhu et al., 2009) were addressed where MS^n was not able to deliver solutions to the problem, as shown in Figure 24.

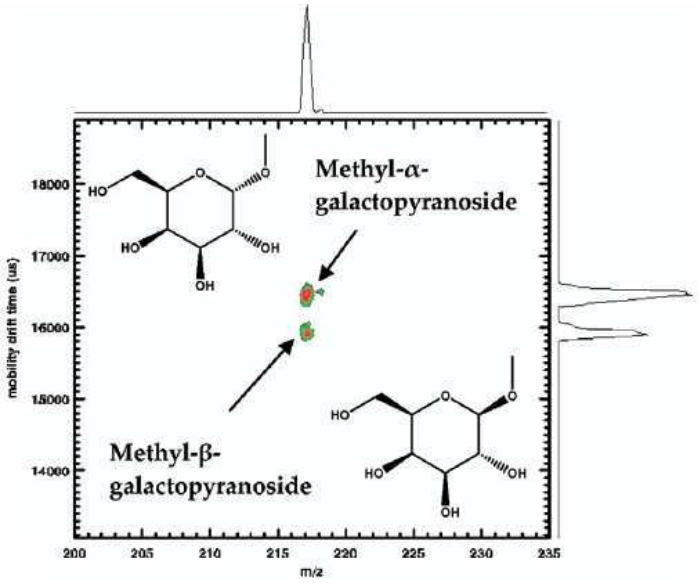

FIGURE 24. Two-dimensional DT-IMS-MS spectra of a mixture of methyl-α and β-D-galactopyranosides showing the separation (N_2 drift gas) of the sodium adducts at m/z 217, adapted from Dwivedi et al. (2007).

H. Rapid analyte testing in complex drug formulations by IMS-MS

The combination of IMS-MS with ambient ionisation mass spectrometry may enable rapid analysis for complex mixtures including drug formulations without laborious method development and consumables required by other separation methods such as 2D LC-MS etc.

The complementary techniques of IMS and DART ambient ionisation operated separately has been demonstrated for AG-013736 in 1 mg Axitinib tablets (Likar et al., 2011), enabling a rapid analysis of AG-013736 in AG-013736 drug substances by DART ionisation and analysis of low-level limits for absence of the drug in placebo tablets by ion mobility spectrometry using a Model 400B IONSCAN-LS from Smiths Detection Scientific (Danbury, CT).

Hyphenated ambient ionisation IMS-MS and nano-electrospray has been used to analyse:

- pharmaceutical formulations including tablets and creams containing one or more of ranitidine, paracetamol, codeine, anastrozole chlorhexidine and a nicotine-containing skin patch (Weston et al., 2005) using DESI.
- pharmaceutical formulations from tablets containing one or more of timolol, paroxetine, paracetamol and codeine using nano-electrospray ionisation (Budimir et al., 2007).
- pharmaceutical formulations containing one or more of paracetomol, ephedrine, codeine and caffeine from non-bonded reversed-phase thin layer chromatography (RP-TLC) plates by desorption electrospray ionisation (DESI) (Harry et al., 2009).

These examples demonstrate the wide applicability of analyses in various types of formulation illustrating that pre-treatment of samples is not required, rapid analyses can be conducted, whilst maintaining reproducible and robust results.

I. Analysis of supramolecular complexes using IMS-MS

The syntheses of supramolecular complexes that possess photo-optical properties are desired for solar energy capture and conversion, molecular machines, photochemical drugs and fluorescent-based sensors.

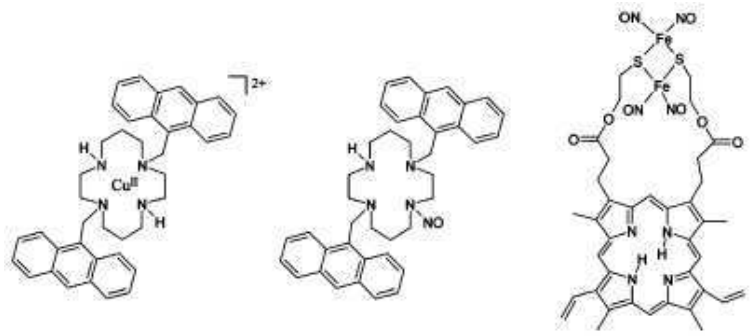

I II III

FIGURE 25. Schematic of $Cu^{2+}(DAC)^{2+}$ (**I**), DAC-NO (**II**), and PPIX-RSE (**III**), adapted from Baker et al., (2005).

DT-IMS-MS was used to probe the structures of bichromic complexes (Figure 25; Baker et al., 2005) in order to provide relevant data for sampling from *in situ* fluid data. Complementary data to ^{1}H-NMR, x-ray crystallography and fluorescence measurements were obtained.

For **I** the crystal structure agreed well with DFT structures and IMS-MS measurements, indicating that solid-state structures agreed well with gas-phase measurements. Only a single peak was observed in the ion mobilogram and calculation gave 161 $Å^2$ as the CCS, compared to 166 $Å^2 \pm 5$ $Å^2$ predicted from the DFT structure.

For **II** DT-IMS-MS measurements indicated two conformers by observation of two main bands in the ion mobilogram, by comparison with computational data this suggested two major families of Up-Up and Up-Down configuration, as shown in FIGURE 6. The solution NMR data for **II** also suggested two conformers but the structures could not be unambiguously determined from the data.

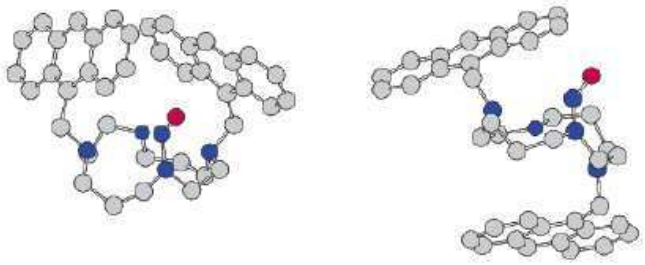

FIGURE 26. Examples of the two families predicted for (**II** + H)$^+$. The Up-Down family is the lower energy family, the Up-Up family has both anthracenyl groups on the same side as the cyclam. Adapted from Baker et al., (2005).

For **III** DT-IMS-MS measurements indicated two conformers which, in combination with DFT measurements indicated two compact structures, rather than folded structures, and correlated well with photophysical features including a bimodal fluorescent decay and a residual emission in steady-state luminescence experiments. The proportion of the two conformers measured by IMS-MS, shown in Figure 27, agreed well with pre-exponential factors that indicated an approximate 80:20 ratio.

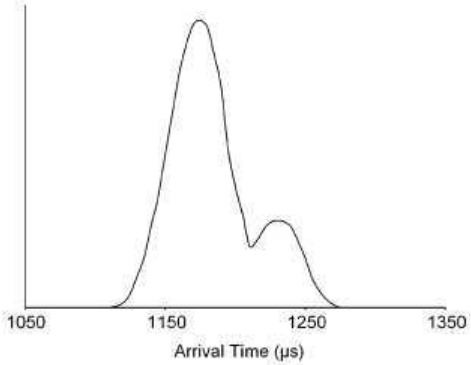

FIGURE 57. ATD for (**III** + H)$^+$ obtained at 80 K. Two distinct peaks indicate two conformers of (**III** + H)$^+$ are present, adapted from Baker et al., (2005).

J. Hydration and desolvation of ligands and substrates

In drug design it is important to consider water molecules particularly in two situations:

(i) those water molecules that will be displaced during ligand binding in a receptor (Poornima and Dean, 1995), and

(ii) those water molecules that will be desolvated crossing the membrane environment.

Water in binding pockets in a receptor can provide surprising entropic and enthalpic contributions to structure and binding affinities (Pace et al., 2004; Homans, 2007). If the key water binding sites and influence of 'small molecule' ligands are known it may be possible to use this information in medicinal drug design, or to predict static hydration sites. It may be especially important to consider bridging waters that link ligand to protein via an extended hydrogen bond network.

Understanding membrane permeability is key to drug delivery and activity and is typically understood by hydrogen bond descriptors such as polar surface area (PSA) and surrogate measurements such as logD. These are considered important physicochemical parameters and modulated during lead optimisation. The reason that these parameters are important is that it is polar groups that are most involved in desolvation when molecules move from an aqueous extracellular environment to the lipophilic membrane environment. During this migration molecules may change their conformation and lose water molecules in order to cross the membrane barrier. To further understand the effect of desolvation on ligands it is possible to add/remove water molecules one by one by changing the water vapour pressure of the DT-IMS-MS cell and gradually ascertain the ion mobility and conformation adopted from a hydrated towards a non-hydrated ion, shown in Figure 28(a). By measuring the energy change at different temperatures a van't Hoff plot can be generated, shown in Figure 28(b), thereby revealing the entropic and enthalpic contributions to hydration.

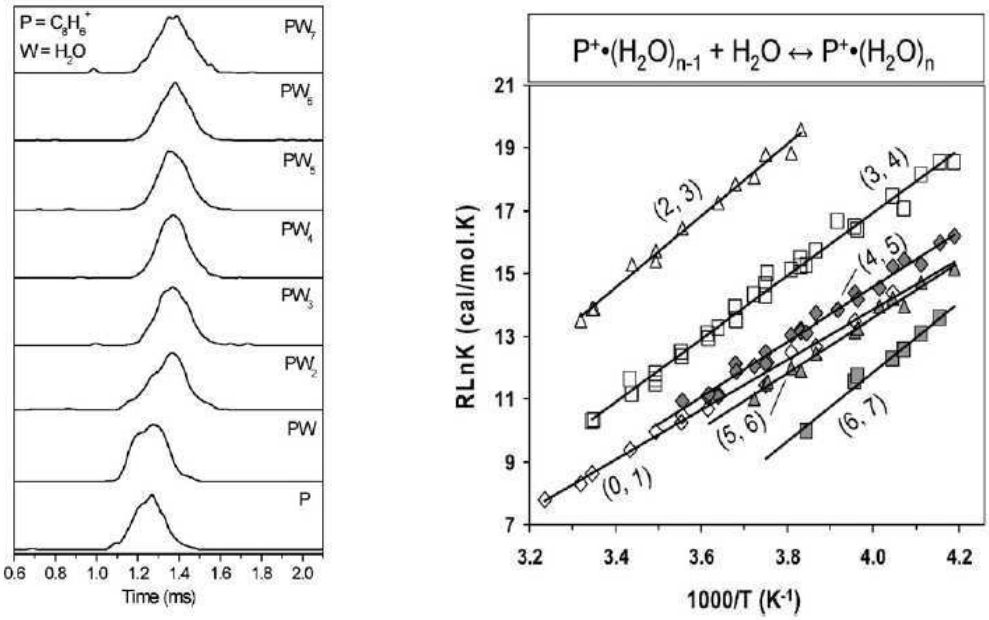

FIGURE 28. (a) ATDs of hydrated phenyl acetylene ions (PW_n) obtained following the injection of the phenyl acetylene ion ($C_8H_6^{\bullet}$+) into 0.34 Torr of water vapor at 249 K (b) Van't Hoff plots for the equilbria $C_8H_6^{\bullet}$+(H_2O)n-1 + H_2O ⇔ $C_8H_6^{\bullet}$+(H_2O)n for n-1 and n as indicated. Adapted from Momoh & El-Shall., (2008).

Hydration of small molecules has been studied for the phenyl acetylene ion, with stepwise hydration energies of 39.7 ± 6.3 kJ mol^{-1} from n=1 to 7; the entropy change for step 7 is larger, indicating a cyclic or cage like water structure (Momoh & El-Shall, 2008). For the benzene ion stepwise hydration energies were 35.6 kJ mol^{-1} from n=1 to 6. The binding energies were larger in the n=7 and 8 clusters indicating cyclic or cage like water structures (Ibrahim et al., 2005). For small protonated peptides the hydration energy is largest for highly charged peptides and small non-arginine containing peptide and typically 30 to 60 kJ mol^{-1} (Wyttenbach et al., 2003); for pentapeptides AARAA, AARAA-OMe and Ac-AARAA the binding energies were typically ~41 kJ mol^{-1}.

The foregoing IMS-MS studies indicate hydration/desolvation studies of small molecule ions can provide structural information in the gas phase, this may be relevant to:

1) understanding water and hydrogen bonded networks (including their entropic consequences) involving protein, ligand and water as part of molecular recognition systems,
2) ligand desolvation on transport through membrane environments, and
3) hydrogen/deuterium exchange experiments and how they are effected by molecular conformation.

Other methods to measure the hydration of small drug-like molecules include infra-red data recorded from a hydrated electrospray source or a droplet ion source (Poully et al., 2008) but these have not always provided unambiguous data, possibly due to the lack of energy required for proton transfer. The measurement of hydration/desolvation energies, described above, may provide a unique insight into the energy landscape of hydration/desolvation by conducting measurements over a range of temperatures.

V. OVERVIEW OF COLLISION CROSS-SECTION (CCS) MEASUREMENTS FOR SMALL MOLECULES

In DT-IMS-MS and TWIMS-MS, larger ions (with a larger CCS) tend to migrate slower through the gaseous medium in the IMS cell compared to smaller ions due to a higher number of collisions with the gas molecules (typically an inert gas such as nitrogen). The drift times through the IMS cell can also reveal structural information such as size, shape and topology; potentially including information

relating to accessible conformations. Unfortunately DMS and FAIMS are, currently, not suitable for carrying out CCS measurements.

Understanding small molecule structure in the gas-phase may be advantageous for quality control or for a more detailed understanding of molecular structure in the gas-phase. For example in drug discovery the physicochemical and binding properties of small molecules depend on their 3D structure and at physiologically relevant temperatures a conformationally flexible small molecule is expected to be able to access a number of energetically feasible conformers, an example is shown in Figure 29. The timescale of interconversion of conformers will define the structural information that can be obtained in solution and in the gas-phase. Understanding the energetics of small molecule conformers is currently largely carried out by generating potential conformers, known as conformational sampling, in computational studies (Foloppe & Chen, 2009).

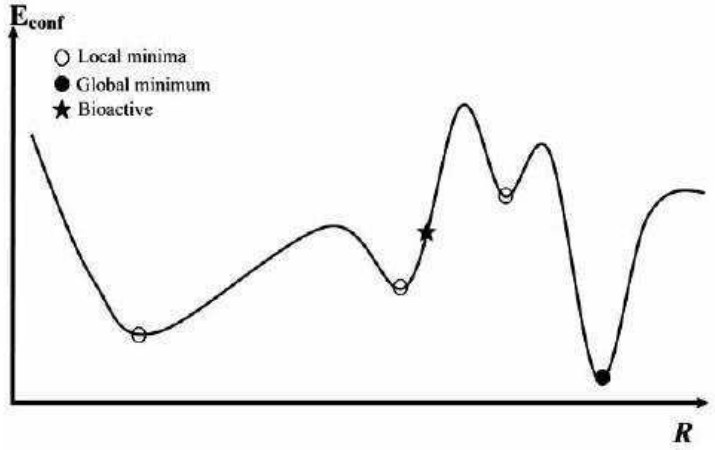

FIGURE 29. Hypothetical example of a one-dimensional molecular conformational potential energy surface. Conformational degrees of freedom (R) are shown on the X axis. Adapted from Foloppe & Chen (2009).

Computationally sampled models have been compared with x-ray crystallographic structures to understand how well the conformer models correlate with the bioactive conformation. Solution NMR can provide valuable information about the 3D structure; however the interpretation is often difficult due to the exchange between several conformations and typically requires molecular modelling to interpret results.

Rapid calculation of CCS by IMS-MS may be useful to decide which molecules in a library (series) could provide the optimum activity. This could be achieved coarsely by excluding molecules which are too rigid/flexible or too big/small as suggested by Williams et al. (2009a). These experiments potentially have the advantage of rapid speed of experiment and low consumption of sample relative to NMR and x-ray techniques. Understanding the conformation in the gas-phase may be a good indicator of the bioactive conformation. This may be especially relevant to compounds in drug discovery which are challenging to isolate and characterise their structure. Mapping the conformational landscape defined via stereo-centres, intramolecular cyclisation etc., may help uncover a path to identification of new target compounds.

For protein structures there is now significant evidence that the gas-phase protein structure can reflect the native state solution phase structure under certain carefully controlled conditions. There have been several publications that demonstrate a good correlation between x-ray, NMR and IMS studies for protein structures (Heck and van den Heuvel, 2004; Rand et al., 2009; Ruotolo et al., 2005; Schultz and Solomon, 1961; Shelimov et al., 1997; Shelimov and Jarrold, 1997), although there have also been some differences noted (Jurneczko and Barran, 2011). However for small molecular weight molecules the evidence that gas-phase structures are similar to solution phase structures has been questioned; in a protein there are multiple cooperative interactions that maintain the 3D structure whereas for a small molecule there are typically fewer interactions resulting in a more flexible structure. Furthermore Allen et al. (1996) compared a range of gas-phase and x-ray molecular substructures for small molecules and suggested that high-energy conformers were represented more in gas-phase, room-temperature Boltzmann distributions than in crystal structures and broad peaks

observed in IMS have generally been interpreted as indicating that multiple conformations are accessible and interconvert on the IMS measurement timescale.

Measurements using IMS-MS may not be the same as NMR (which are subject to solvent effects) or x-ray (which are subject to crystal lattice effects). In enzymes and membrane receptors, biomolecular recognition processes are likely to take place in hydrophobic 'binding pockets' of proteins where there will then be several interactions for a ligand including hydrophobic amino acids, with a large possibility (>0.8) of excluding most water molecules. The dielectric constant of a partial vacuum in IMS-MS (c.f. ε_{vacuum} = 1) is more similar to the immediate environment of a membrane receptor ($\varepsilon_{peptide/protein}$ = 2–4) than for water (ε_{water} = 80)(Bastug and Kuyucak, 2003). We may therefore postulate that the environment of a bioactive conformer will often be intermediate between aqueous and gas-phase (vacuum). Therefore the gas phase may be an appropriate medium in which to study the 'small molecule' structures which in their active form are bound to a receptor located in a membrane, rather than in solution.

A. CASE STUDIES OF COLLISION CROSS-SECTION (CCS) MEASUREMENTS FOR SMALL MOLECULES

1. Study of an organoruthenium complex and its adducts with a DNA oligonucelotide

TWIMS-MS has been used to understand the binding of a "piano-stool" shaped organoruthenium complex with a single stranded oligonucleotide hexamer that show promise as an anti-cancer agent. The illustration in Figure 30 shows examples of the protonated and deprotonated complexes, the doubly positive charged complex and the doubly negative charged complex. The single peak (A) suggests a single species, whereas multiple peaks in (B), (C) and (D) suggest either multiple binding of the Ru-drug fragment (confirmed by interpretation of the mass spectra collected) or different conformers present in the mononucleotide due to different charge distributions along the phosphate backbone (Williams et al., 2009a).

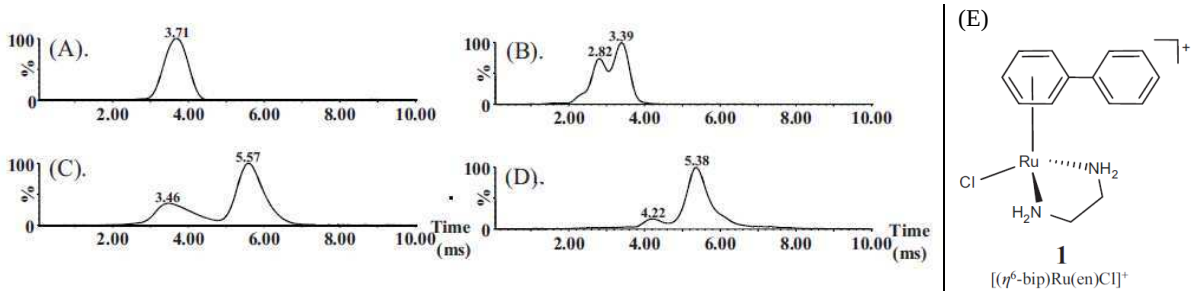

FIGURE 30. Arrival time distributions (ATDs) or drift times for (A) the $[M+2H]^{2+}$ ion of d(CACGTG); (B) the $[M-2H]^{2-}$ ion of d(CACGTG); (C) the complex $[CACGTG+2[(\eta^6\text{-bip})Ru(en)]-2H]^{2+}$; and (D) the complex $[CACGTG+2[(\eta 6\text{-bip})Ru(en)]-6H]^{2-}$ and (E) structure of the organoruthenium anticancer complex ($[(\eta^6\text{-bip})Ru(en)]$), adapted from Williams et al., (2009a).

The CCS values obtained for the Ru-based drug correlated well with those obtained by x-ray crystallographic data so that binding could be easily identified. Using MS/MS experiments, shown in Figure 31, subsequent to IMS separation, enabled the binding site to be determined by examining the resulting fragmentation pattern.

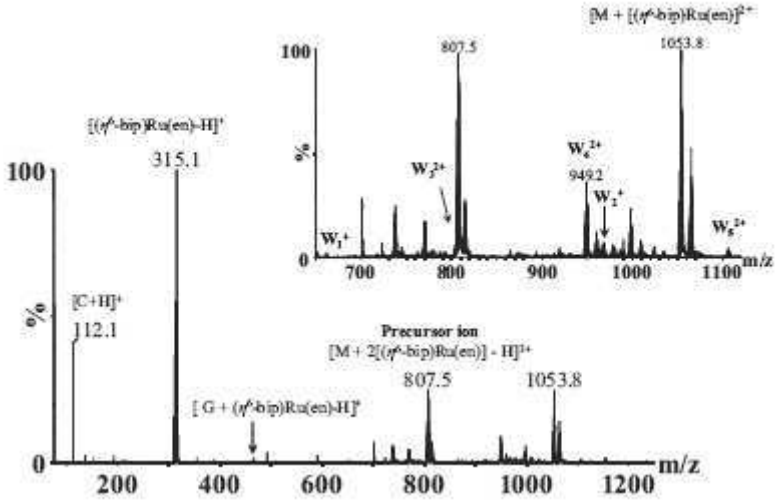

FIGURE 31. MS/MS spectrum of the precursor ion of m/z 807.5, corresponding to [CACGTG+2[(η6-bip)Ru(en)] H]$^{3+.}$ Inset shows the relevant sequence-specific ions detected. (Note: M represents CACGTG), adapted from Williams et al., (2009a).

2. Study of the in-flight epimerisation of a bis-Tröger base

The epimerisation pathway via the proposed alternatives of a) a proton catalysed ring opening or b) retro-Diels-Alder of a bis-Tröger base, shown in Figure 32, were investigated using TWIMS-MS (Révész et al., 2011) as this could be important for the design of Tröger bases which, with their tweezer type structure, have been suggested as useful agents as molecular receptors, chiral solvating agents and inclusion complexes (Maitra et al., 1995).

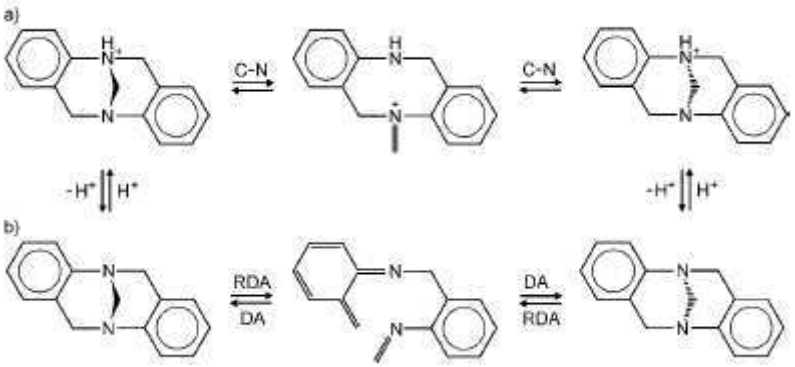

FIGURE 32. Proposed mechanism for epimerisation of a Tröger base by a) a proton catalysed ring opening or b) a retro-Diels-Alder mechanism, Révész et al., (2011).

The two structures were separated well in the gas-phase TWIMS stage (FIGURE 33) and activation of ions pre-TWIMS separation and post-TWIMS separation demonstrated that the anti-1H$^+$ isomer is the most thermodynamically favoured by measuring the intensity of each parent ion. The preferred mechanism was also concluded to be the proton catalysed ring opening as demonstrated by the lack of epimerisation when a Na$^+$ Tröger base was used as a surrogate proton-like participant in the reaction, thus eliminating the possibility of a retro-Diels-Alder mechanism.

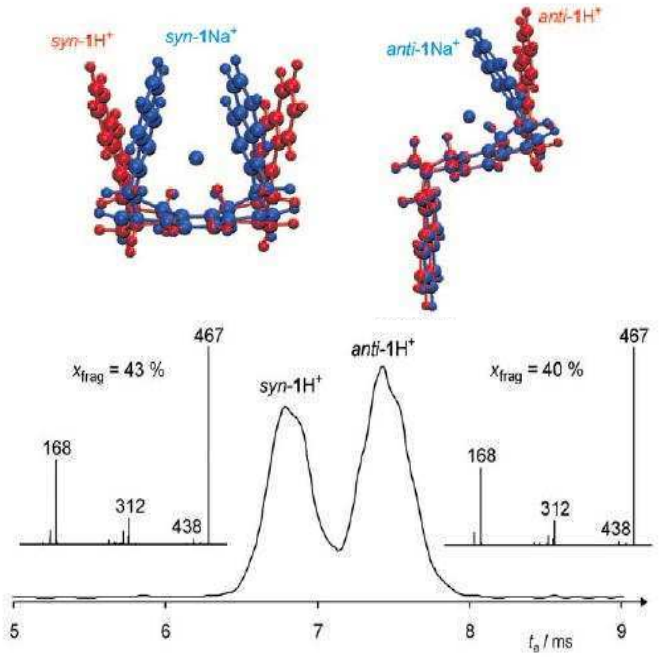

FIGURE 33. Ion mobility trace with associated mass spectra (shown inset) of the *anti-* and *syn-* isomers. The computationally calculated structures are shown above, adapted from Révész et al., (2011).

B. Measurement of collision cross-section (CCS) for small molecules using DT-IMS-MS

The measurement of CCS in DT-IMS is simplified by the use of a static, uniform, electric field in which ion motion takes place; the physical principles are established and mobility values can be used to derive the collision cross-section. Knowing the length of the drift region and the time that ions take to traverse it enables the ion's velocity to be determined:

$$v = \mathrm{KE} \rightarrow \frac{\mathrm{L}}{\mathrm{t_d}} = \mathrm{K}\frac{\mathrm{V}}{\mathrm{L}} \rightarrow \mathrm{K} = \frac{\mathrm{L}^2}{\mathrm{Vt_d}} \qquad (9)$$

where v is the ion's velocity, K is the ion mobility constant, E is the electric field, L is the length of the drift tube, t_d is the arrival time and V is the voltage across the drift region.

K should be corrected for temperature and pressure to obtain the reduced ion mobility, K_0 (corrected to 273 K and 760 Torr):

$$\mathrm{K_0} = \mathrm{K}\left[\frac{273}{\mathrm{T}}\right]\left[\frac{\mathrm{P}}{760}\right] \qquad (10)$$

The collision cross-section, Ω_T, can then be derived directly:

$$\Omega_{\mathrm{T}} = \left(\frac{3ze}{16N}\right)\left(\frac{2\pi}{\mu kT}\right)^{1/2}\left(\frac{1}{K}\right) \qquad (11)$$

where Ω is the collision cross-section, ze is the ionic charge, N is the background gas number density, μ is the reduced mass of the ion-neutral pair, k is Boltzmann's constant, T is the gas temperature and

K is the mobility constant.

C. Calculation of collision cross-section (CCS) for small molecules using TWIMS

The measurement of CCS in TWIMS is not typically directly derived from the mobility of an ion (Giles et al., 2010) as the motion of the analyte in the travelling wave regime is complicated and, to date, is not fully understood. The TWIMS system is, therefore, usually calibrated using ions that have previously been measured by employing DT-IMS. A typical calibration regime (Knapman et al., 2010) has been described based on the CCSs of oligo-glycine ions (available at http://www.indiana.edu/~clemmer/) which are currently accepted to be suitable as they are high mobility ions in the expected mobility range of small molecules, and have been measured previously using DT-IMS. Calibration with a static 4 V wave gave more drift time values over a narrower range of CCSs than a wave ramp, potentially resulting in greater resolving power. Although changes can be made to the buffer gas used in the measurement, the larger the buffer gas molecules, the larger the CCS and it was noted that the buffer gas radius used in theoretical calculations must be indicative of the buffer gas used in the original DT-IMS measurements (typically helium), even if the analysis of calibrants and analytes is carried out in a different buffer gas.

The experimental resolving power was reported under these conditions for the isomeric amino acids isoleucine and leucine (131 Da), calculated the CCS at 68.95 $Å^2$ and 70.51 $Å^2$, respectively from the measured arrival time distributions (see Figure 34).
.

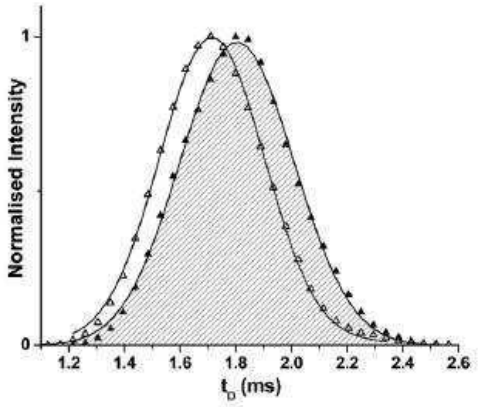

FIGURE 64. Overlaid mobility chromatograms of L-Ile (open) and L-Leu (filled) acquired using a static 4 V wave height. The ESI-TWIMS-MS experimental CCS values measured were 68.95 and 70.51$Å^2$, and the calculated CCS values were 70.81 and 72.03$Å^2$, for L-Ile and L-Leu, respectively. Adapted from Knapman et al., (2010).

To understand the differences between solution state and gas-phase measurements the theoretical collision cross-sections were calculated as a weighted average over multiple solution-phase rotameric states from a database of 5000 protein structures and compared to the experimentally measured gas-phase values (Table 4). Calculated CCS values for hydrophobic amino acids gave the best agreement with gas-phase TWIMS values, whilst more polar residues are experimentally found to be much smaller than calculated, mostly likely due to burying of polar and charged termini. The largest differences also appear to be correlated to the degrees of freedom in the amino acid side-chain.

TABLE 4. Comparison of measured and predicted CCS values for seven amino acids, adapted from Knapman et al., (2010).

Amino acid	Mw (Da)	Rotamers	TWIMS experimental CCS ($Å^2$)	CCS predicted from solution state ($Å^2$)	Difference ($Å^2$)	Notes
Pro	115.12	2	62.43	63.16	0.73	Hydrophobic
Val	117.15	3	64.81	64.82	0.01	Hydrophobic
Leu	131.12	4	70.51	72.03	1.52	Hydrophobic
Ile	131.12	4	68.95	70.81	1.86	Hydrophobic
Asp	133.11	5	62.93	69.81	6.88	Polar

Gln	146.15	5	62.85	75.08	12.23	Polar
Glu	147.13	7	63.35	76.69	13.34	Polar

This demonstrates that IMS-MS can distinguish between subtle changes in shape e.g. differentiating Leu and Ile and also has the potential to reveal structural information about the important interactions present in the gas-phase such as the burial of the polar groups in the examples Gln and Glu.

D. Calculation of collision cross-section (CCS) for small molecules using overtone IMS-MS

Recently, overtone mobility spectrometry (Kurulugama et al., 2009; Valentine et al., 2009), where separation is achieved by applying time-dependent electric fields to sequential segments in a drift-tube thus eliminating ions that are not resonant with the applied field, has been used to demonstrate measurements of ion collision cross-sections:

$$\Omega = \frac{(18\pi)^{1/2}}{16} \frac{ze}{(k_b T)^{1/2}} \left[\frac{1}{m_I} + \frac{1}{m_B} \right]^{1/2} \frac{E[\phi(h-1)+1]}{f(l_t + l_e)} \frac{760}{P} \frac{T}{273.2} \frac{1}{N} \quad (12)$$

where Ω is the collision cross-section, k_b is the Boltzmann constant, z is the ionic charge, e is the charge of an electron, N is the buffer gas density, T is the temperature of the buffer gas, P is the pressure of the buffer gas, E is the electric field, m_I and m_B are the masses of the ion and the buffer gas. The overtone IMS specific parameters include f which is the application frequency, h is the harmonic index, l_t is the ion transmission length and l_e is the ejection length.

Reduced ion mobilities are reported to enable a comparison of DT-IMS-MS and overtone-IMS-MS measurements and are, in general, in good agreement. An especially interesting feature is the potential for overtone-IMS-MS to exclude different ion structures i.e. with different ion mobilities in the IMS stage. Typical IMS and TWIMS approaches are thought to measure an experimental average of all structures sampled within the IMS drift time, whereas overtone-IMS-MS appears to enable selection of particular structures over the IMS drift-time, potentially giving a better understanding of transitions on the IMS measurement timescale, in the order of a few milliseconds. Current measurements are limited for small molecules but development is ongoing.

E. Using theoretical calculations to understand ion mobility data

The assignment of structural information is typically made by comparing theoretical, calculated CCS values with experimentally determined CCS values by using the following procedures:

1. generate list of conformers,
2. minimise structures to lowest energy structures,
3. calculation of theoretical CCS, and
4. comparison of theoretical CCS values with experimentally determined values.

1. Generate list of conformers

Initially the molecule must be transformed from a flat 2D to a representative 3D structure at physiological pH taking into account tautomerism, likely protonation site(s), bond lengths etc. The accessible conformations can be explored for small molecules (Dear et al., 2010; Williams et al., 2009b) using methods including systematic search, molecular dynamics, random search and grid search tools but may be very computationally expensive if the number of rotatable bonds is high, requiring evaluation of thousands of potential structures for relatively simple structures.

2. Minimise structure to lowest energy structures

Molecular dynamics approaches have been applied to small molecules with success and computationally are far less demanding than for large molecules (Baumketner et al., 2006; von Helden et al., 1995; Hoaglund-Hyzer et al., 1999; Jarrold, 2000; Kinnear et al., 2002). Methods have included force-field techniques including MMFF94 forcefield (Dear et al., 2010) and CHARM (Mao et al., 2001) but quantum mechanical methods e.g., density functional theory (DFT) may also be feasible for understanding small molecule structures. Indeed DFT has almost become the 'norm' for

calculating ion structures (Holmes et al., 1985), as it is more accurate than semi-empirical methods . Recent work (Alex et al., 2009; Wright et al., 2010) has highlighted the potential for DFT to understand electron density in bond formation/cleavage and the effect of protonation on bond lengths, which makes DFT a potentially powerful tool in modelling ion structures in IMS-MS. Indeed the information obtained from DFT calculations may contribute to a better understanding of the ion structure for both the IMS separation and any tandem MS results.

3. Calculation of theoretical CCS

The main calculation protocols for obtaining theoretical CCS values in IMS include projection approximation (PA), trajectory method (TJ) and exact hard sphere scattering (EHSS). Whilst there has been some debate about which type of modelling is most appropriate, it is generally recommended to use the projection approximation (PA) method for small molecules of 20-100 atoms, for example using the Sigma software package or MOBCAL software. However, PA typically underestimates collision cross-sections for polyatomic species, especially for different surfaces including concave structures, by up to 20% (Shvartsburg and Jarrold, 1996), so is not typically recommended for larger molecular weight structures.

TJ typically works well for any size system, but calculations are computationally expensive. Exact Hard Sphere Scattering (EHSS) typically fails with small molecules because the ion-buffer gas interaction becomes important compared to the geometry of the ion and careful calibration of the relevant atomic radii is essential (Shvartsburg and Jarrold, 1996). EHSS and TJ appear to provide better agreement for larger molecular weight ions as the parameterisation of EHSS is based on fullerenes and other large molecular weight ions.

There have been attempts to improve modelling, for large molecules (Shvartsburg et al., 2007) and small molecules (Knapman et al., 2010; Siu et al., 2010), by construction of new parameter basis sets with values for the carbon, oxygen, helium and nitrogen interaction radius calculated from suitable representative molecules. Further development of modelling and prediction techniques (Fernandez-Lima et al., 2009) and improvement in parameter basis sets may well provide closer agreement between calculated and measured CCSs. Recent improvements to a nitrogen based trajectory method (Campuzano et al. 2011) may help understand data generated in $N_{2(g)}$ (as the less polarizable $He_{(g)}$ is typically used) and create better calibrations for collision cross sections (especially useful in TWIMS where $N_{2(g)}$ is the typical drift gas). The set of collision cross sections for pharmaceutically relevant 'small molecule' compounds appears self consistent (R^2 = 0.9949) and covers a useful range of 124.5 to 254.3 $Å^2$ for nitrogen gas and a range of 63.0 to 178.8 $Å^2$ for helium gas.

4. Comparison of calculated CCS values with experimentally determined values

Typically validation is best achieved using known standards within experimental sets, either for relative ranking of results or to increase confidence in measurements. Structure co-ordination sets are widely available for some species e.g. at the RCSB Protein Data Bank and have been data based by Clemmer (available at http://www.indiana.edu/%7eclemmer/Research/cross%20section%20database/Proteins/protein_cs.htm). However, it should be noted that the co-ordination structures from different sources may not agree as NMR structures are often subject to solvent effects, x-ray structures subject to crystal lattice effects and measurements by ion mobility may be subject to gas-phase neutral contamination, ionisation and solvent effects. Some publications describe the calculation of theoretical collision-cross sections using datasets obtained from NMR and x-ray files (e.g. PDB files) as input without subsequent energy minimisation in the gas-phase which could result in erroneous estimates of CCS and further assignment; in such a case a better understanding via structure/energy minimisation may be important.

VI. PREDICTION OF ION MOBILITY CONSTANTS

Whilst many approaches to IMS explicitly use or attempt to derive information on the 3D structure of the ion another approach is to use molecular descriptors to adequately describe an ion and predict the reduced mobility without any requirement to carry out computationally expensive geometry optimisation. A quantitative structure property relationship (QSPR) methodology using five descriptors for a training set of 70 organic compounds and excluding three outliers gave a multi-linear regression (MLR) of R^2 = 0.98 and s = 0.047; the test set of seven compounds gave s = 0.047 (Wessel and Jurs, 1994). Later, using six molecular descriptors on a training set of 135 compounds and testing the model with 18 compounds gave an RMS error of 0.038 (Wessel et al., 1996). A more

diverse set of 182 compounds and modification of two of the descriptors correlated with an R^2 =0.80 (Agbonkonkon et al., 2004). A subset of 159 of that data set was used to develop linear and non-linear models using MLR and progression pursuit regression to achieve R^2 values of 0.908 and 0.938 and s = 0.066 and 0.055, respectively (Liu et al., 2007a). The recent formulation of a linear equation for ion mobility in a series of polar aliphatic organic compounds resulted in ion mobility predictions that were typically >99% accurate (Hariharan et al., 2010).

These molecular descriptor approaches are now widely used in predicting peptide IMS-MS drift times (Wang et al., 2010) to improve confidence in peptide identification. The same approach to prediction of 'small molecule' IMS-MS drift times could well help refine models of drift time prediction and better understand important interactions affecting drift time and thus gas-phase structures, however this is currently not well understood.

VII. FUTURE DEVELOPMENTS

The adoption of IMS-MS both for small molecule as well as large molecule applications is likely to continue strongly, assisted by rapid developments in IMS design that marries the two stages of IMS and MS and mitigates the challenges of ion efficiency and resolution that has hindered their combination.

The resistive glass-IMS design recently invented to replace the traditional stacked-ring ion guides enables easier construction (Kwasnik and Fernández, 2010) and designs include a segmented rf quadrupole in the vacuum interface that improve sensitivity by over 2 order of magnitude (Kaplan et al., 2010). The inverse ion mobility spectrometry technique that applies an inverted pulse to the shutter grid appears to increase resolution by 30-60% presumably by creating a gap in the charge cloud and thus reducing space-charging effects (Tabrizchi and Jazan, 2010).

A further hyphenation of a photoelectron spectrometer to a IMS-TOFMS shows promise as a complementary method to obtain further information on the structures of gas-phase ions by obtaining photoelectron spectra at three different detachment laser wavelengths (Vonderach et al., 2011), and also hints at the possibilities for further information-rich data to be acquired and combined with IMS-MS by further hypenation.

The adoption of IMS in hyphenated IMS-MS systems is continuing with important developments, for example, Agilent previously announced collaborations with Owlstone Nanotechnologies for an IMS-MS system and Bruker have investigated new modes of IMS (Baykut et al., 2009). There have been long-term research investments demonstrated in the launch of the second generation Waters Synapt G2 IMS-MS with improved resolution and ion transmission and with the AB Sciex SelexION technology that is available for the AB Sciex Triple Quad 5500 and QTRAP 5500 Systems including selection of gas-phase dopants which can improve IMS separation and rapid 25 ms cycle time per MRM which matches cycle times with multi-component analysis and UHPLC time scales.

VIII. CONCLUSIONS

Whilst IMS is a ubiquitous technique in airports as well as military and forensic applications, it is still the case that using IMS-MS for measuring structural information and for separations in 'small molecule' applications there are subtle differences that can significantly affect the mobility and there is much more to be understood about how to measure the structures of gas-phase ions reliably, the nature of the fundamental intra-molecular interactions that define the structures and what the effect of ion-neutral interactions are on ion mobility.

Many chemical classes have been investigated using IMS and IMS-MS and some of the main publications are listed in Table 5 to direct the reader to more detail on those classes.

TABLE 5. Applications of IMS-MS and IMS to 'small molecule' classes.

Class	Year
Hydrocarbons (Creaser et al., 2004)	1973
Halogenated benzenes and nitro benzenes (o-, m-substituted) (Karpas et al., 1988)	1973
Dihalogenated benzenes (o-, m-substituted) (Karpas et al., 1988)	1974

Benzoic and isophthalic and phthalic acids (Karpas et al., 1988)	1975
Some sec-butylcholorodiphenyl oxides (Karpas et al., 1988)	1976
o- and p- substituted chlorodiphenyl oxides (Karpas et al., 1988)	1976
Ethyl butyl esters of maleic and fumaric (Karpas et al., 1988)	1982
Succinic acids (Karpas et al., 1988)	1982
Isomeric ketones 2-octanone vs. 4,4-dimethyl-3-hexanone (Karpas et al., 1988)	1986
Isomeric alcohols 1-octanol vs. 2-octanol (Karpas et al., 1988)	1986
Substituted electrophilic olefins, keto enol isomers, 2 keto and 2 enol (Karpas et al., 1988)	1988
Amides and amines (Karpas et al., 1988) (Karpas et al., 1994)	1989 & 1994
Anilines (Karpas et al., 1990b)	1990
Simple monocyclic and dicyclic compounds (Karpas et al., 1990a)	1990
Aminoazoles (Karpas and Tironi, 1991)	1991
Ketones (Karpas, 1991)	1991
Aminoalcohols (Karpas, 1992)	1991
Benzodiazepines, amphetamines and opiates (Karpas et al., 1988)	2001 & 2002
Amino acids (Asbury & Hill, 2000b)	2001
Amphetamines (Matz and Hill, 2002)	2002

Standardized calibration and measurement methods (Fernández-Maestre et al., 2010b), easily implemented and accurate predictive models and interpretation of results are still being developed but show great promise. The interchange between academia, vendors and industry is ensuring more options are available to potential users of IMS-MS. A range of current commercial manufacturers and IMS-MS types are listed in Table 6 for reference.

TABLE 6. Commercially available IMS systems, or accessories able to interface to MS systems.

IMS-MS manufacturer	**Type**
Excellims IMS-MS	DT-IMS
Tofwerk IMS-MS	DT-IMS
Waters Synapt IMS-MS	TWIMS
Thermo FAIMS cylindrical electrode	FAIMS
Owlstone Nanotech	FAIMS
AB Sciex SelexION parallel plate	DMS
Sionex microDMx	DMS

Over the last decade there have been many novel applications and developments in IMS-MS involving new methods to generate ions, accumulate and focus ions, select ions preferentially, measure and process the multiplexed information and they have been used to solve problems ranging from hydration/desolvation in 'small' organic molecules to understanding the fundamental interactions in the building blocks of life, amino acids. IMS-MS is a novel method that can separate ions and use information on their mobility to assign structure on an unparalleled rapid timeframe and at high levels of sensitivity. In combination with a range of analytical equipment including ionisation sources, separation devices, solution chemistry and gas-phase chemistry; the use of IMS-MS offers a versatile and powerful approach to unique insights into complex mixtures and hitherto ambiguous structures.

REFERENCES

Agbonkonkon N, Tolley HD, Asplund MC, Lee ED, Lee ML. 2004. Prediction of gas-phase reduced ion mobility constants (K0). Anal Chem 76:5223-5229.

Aksenov AA, Kapron JT. 2010. Behaviour of tetraalkylammonium ions in high-field asymmetric waveform ion mobility spectrometry. Rapid Commun Mass Spectrom 24:1392-1396.

Albritton DL, Miller TM, Martin DW, McDaniel EW. 1968. Mobilities of mass-identified $H3^+$ and H^+ ions in hydrogen. Phys Rev 171:94.

Alex A, Harvey S, Parsons T, Pullen FS, Wright P, Riley, JA. (2009). Can density functional theory (DFT) be used as an aid to a deeper understanding of tandem mass spectrometric fragmentation pathways?. Rapid Commun Mass Spectrom, 23: 2619–2627

1307 Allen FH, Harris SE, Taylor R. 1996. Comparison of conformer distributions in the crystalline state
1308 with conformational energies calculated by *ab initio* techniques. J Comput-Aid Mol Des
1309 10:247-254.
1310 Alonso R, Rodríguez-Estévez V, Domínguez-Vidal A, Ayora-Cañada MJ, Arce L, Valcárcel M. 2008.
1311 Ion mobility spectrometry of volatile compounds from iberian pig fat for fast feeding regime
1312 authentication. Talanta 76:591-596.
1313 Project Summary. . Recovery.gov.
1314 http://www.recovery.gov/Transparency/RecipientReportedData/pages/RecipientProjectSumm
1315 ary508.aspx?AwardIDSUR=93260&qtr=2010Q3.
1316 Arthur KE, Wolff J. Carrier DJ. 2004. Analysis of betamethasone, dexamethasone and related
1317 compounds by liquid chromatography/electrospray mass spectrometry. Rapid Commun Mass
1318 Spectrom 18: 678-684
1319 Asbury GR, Hill HH. 2000a. Evaluation of ultrahigh resolution ion mobility spectrometry as an
1320 analytical separation device in chromatographic terms. J. Micro Sep 12:172-178.
1321 Asbury GR, Hill HH. 2000b. Separation of amino acids by ion mobility spectrometry. J Chromatog A
1322 902:433-437.
1323 Asbury GR, Hill HH. 2000c. Using Different Drift Gases To Change Separation Factors (α) in Ion
1324 Mobility Spectrometry. Anal. Chem.72: 580-584
1325 Aston FW. 1919. A positive ray spectrograph. Philos. Mag., 38: 707-715.
1326 Baim MA, Hill HH. 1982. Tunable selective detection for capillary gas chromatography by ion mobility
1327 monitoring. Anal Chem 54:38-43.
1328 Baker ES, Bushnell JE, Wecksler SR, Lim MD, Manard MJ, Dupuis NF, Ford PC, Bowers MT. 2005.
1329 Probing shapes of bichromophoric metal−organic complexes using ion mobility mass
1330 spectrometry. J Am Chem Soc 127:18222-18228.
1331 Barnes WS, Martin DW, McDaniel EW. 1961. Mass spectrographic identification of the ion observed
1332 in hydrogen mobility experiments. Phys. Rev Lett 6:110.
1333 Bastug T, Kuyucak S. 2003. Role of the dielectric constants of membrane proteins and channel water
1334 in ion permeation. Biophys J 84:2871-2882.
1335 Baumketner A, Bernstein SL, Wyttenbach T, Lazo ND, Teplow DB, Bowers MT, Shea J-E. 2006.
1336 Structure of the 21-30 fragment of amyloid β-protein. Protein Sci 15:1239-1247.
1337 Baykut G, von Halem O, Raether O. 2009. Applying a Dynamic Method to the Measurement of Ion
1338 Mobility. J Am Soc Mass Spectrom, 20: 2070-2081
1339 Beegle LW, Kanik I, Matz L, Hill HH. 2001. Electrospray ionization high-resolution ion mobility
1340 spectrometry for the detection of organic compounds, 1. amino acids. Anal Chem 73:3028-
1341 3034.
1342 Belov ME, Clowers BH, Prior DC, Danielson III WF, Liyu AV, Petritis BO, Smith RD. 2008.
1343 Dynamically multiplexed ion mobility time-of-flight mass spectrometry. Anal Chem 80:5873-
1344 5883.
1345 Bluhm BK, Gillig KJ, Russell DH. 2000. Development of a fourier-transform ion cyclotron resonance
1346 mass spectrometer-ion mobility spectrometer. Rev Sci Instrum 71:4078.
1347 Bohrer BC, Merenbloom SI, Koeniger SL, Hilderbrand AE, Clemmer DE. 2008. Biomolecule analysis
1348 by ion mobility spectrometry. Ann Rev Anal Chem 1:293-327.
1349 Budimir N, Weston DJ, Creaser CS. 2007. Analysis of pharmaceutical formulations using atmospheric
1350 pressure ion mobility spectrometry combined with liquid chromatography and nano-
1351 electrospray ionisation. Analyst 132:34.
1352 Buryakov IA, Krylov EV, Nazarov EG, Rasulev UK. 1993. A new method of separation of multi-atomic
1353 ions by mobility at atmospheric pressure using a high-frequency amplitude-asymmetric strong
1354 electric field. Int J Mass Spectrom. 128:143-148
1355 Canterbury JD, Yi X, Hoopmann MR, MacCoss MJ. 2008. Assessing the dynamic range and peak
1356 capacity of nanoflow lc−faims−ms on an ion trap mass spectrometer for proteomics. Anal
1357 Chem 80:6888-6897.
1358 Campuzano I, Bush MF, Robinson CV, Beaumont C, Richardson K, Kim H, Kim HI. 2012. Structural
1359 Characterization of Drug-like Compounds by Ion Mobility Mass Spectrometry: Comparison of
1360 Theoretical and Experimentally Derived Nitrogen Collision Cross Sections. Anal Chem 84
1361 (2):1026–1033.
1362 Champarnaud E, Laures AM-F, Borman PJ, Chatfield MJ, Kapron JT, Harrison M, Wolff J-C. 2009.
1363 Trace level impurity method development with high-field asymmetric waveform ion mobility
1364 spectrometry: systematic study of factors affecting the performance. Rapid Commun Mass
1365 Spectrom 23:181-193.

Clemmer DE. 1997. Injected-ion mobility analysis of biomolecules. http://www.indiana.edu/~clemmer/Publications/pub%20042.pdf.
Clowers BH, Ibrahim YM, Prior DC, Danielson WF, Belov ME, Smith RD. 2008. Enhanced ion utilization efficiency using an electrodynamic ion funnel trap as an injection mechanism for ion mobility spectrometry. Anal. Chem 80:612-623.
Clowers BH, Hill HH. 2006. Influence of cation adduction on the separation characteristics of flavonoid diglycoside isomers using dual gate-ion mobility-quadrupole ion trap mass spectrometry. J Mass Spectrom 41:339-351.
Clowers BH, Siems WF, Hill HH, Massick SM. 2006. Hadamard transform ion mobility spectrometry. Anal Chem 78:44-51.
Collins DC, Lee ML. 2001. Electrospray ionization gas-phase electrophoresis under ambient conditions and it's potential or high-speed separations. Fresenius' J Anal Chem 369:225-233.
Covey T, Douglas DJ. 1993. Collision cross sections for protein ions. J. Am. Soc. Mass Spectrom.4: 616-623

Coy SL, Krylov EV, Schneider BB, Covey TR, Brenner DJ, Tyburski JB, Patterson AD, Krausz KW, Fornace AJ, Nazarov EG.2010.Detection of Radiation-Exposure Biomarkers by Differential Mobility Prefiltered Mass Spectrometry (DMS-MS). Int. J. Mass Spectrom.. 291: 108-117
Creaser CS, Benyezzar M, Griffiths JR, Stygall JW. 2000. A tandem ion trap/ion mobility spectrometer. Anal Chem 72:2724-2729.
Creaser CS, Griffiths JR, Bramwell CJ, Noreen S, Hill CA, Thomas CLP. 2004. Ion mobility spectrometry: a review. part 1. structural analysis by mobility measurement. Analyst 129:984.
Cui M, Ding L, Mester Z. 2003. Separation of cisplatin and its hydrolysis products using electrospray ionization high-field asymmetric waveform ion mobility spectrometry coupled with ion trap mass spectrometry. Anal Chem 75:5847-5853.
Cuyckens F, Wassvik C, Mortishire‐Smith RJ, Tresadern G, Campuzano I, Claereboudt J. 2011. Product ion mobility as a promising tool for assignment of positional isomers of drug metabolites. Rapid Commun Mass Spectrom. 25:3497-3503
D'Agostino PA, Chenier CL. 2010. Desorption electrospray ionization mass spectrometric analysis of organophosphorus chemical warfare agents using ion mobility and tandem mass spectrometry. Rapid Commun Mass Spectrom 24:1617-1624.
Dear GJ, Munoz-Muriedas J, Beaumont C, Roberts A, Kirk J, Williams JP, Campuzano I. 2010. Sites of metabolic substitution: investigating metabolite structures utilising ion mobility and molecular modelling. Rapid Commun Mass Spectrom 24:3157-3162.
de la Mora JF, Ude S, Thomson BA. 2006. The potential of differential mobility analysis coupled to MS for the study of very large singly and multiply charged proteins and protein complexes in the gas phase. Biotechnol. J. 1: 988-997
Douglas DH. 1998. Applications of Collision Dynamics in Quadrupole Mass Spectrometry. J Am Soc Mass Spectrom. 9: 101-113
Dussy FE, Berchtold C, Briellmann TA, Lang C, Steiger R, Bovens M. 2008. Validation of an ion mobility spectrometry (ims) method for the detection of heroin and cocaine on incriminated material. Forensic Sci Int 177:105-111.
Dwivedi P, Bendiak B, Clowers BH, Hill HH. 2007. Rapid resolution of carbohydrate isomers by electrospray ionization ambient pressure ion mobility spectrometry-time-of-flight mass spectrometry (esi-apims-tofms). J Am Soc Mass Spectrom 18:1163-1175.
Dwivedi P, Schultz AJ, Jr HHH. 2010. Metabolic profiling of human blood by high-resolution ion mobility mass spectrometry (im-ms). Int J Mass Spectrom 298:78-90.
Dwivedi P, Wu C, Matz LM, Clowers BH, Siems WF, Hill HH. 2006. Gas-phase chiral separations by ion mobility spectrometry. Anal Chem 78:8200-8206.
Eatherton RL, Morrissey MA, Siems WF, Hill HH. 1986. Ion mobility detection after supercritical fluid chromatography. J High Res Chromatogr 9:154-160.
Eiceman GA, Karpas Z. 2004. Ion mobility spectrometry. 2nd edition. Boca Raton, FL, USA: CRC Press
Eiceman GA, Yuan-Feng W, Garcia-Gonzalez L, Harden CS, Shoff DB. 1995. Enhanced selectivity in ion mobility spectrometry analysis of complex mixtures by alternate reagent gas chemistry. Anal Chim Acta 306:21-33.
Eiceman GA, Krylov EV, Krylova NS, Nazarov EG, Miller RA. 2004. Separation of Ions from Explosives in Differential Mobility Spectrometry by Vapor-Modified Drift Gas. Anal. Chem. 76: 4937-4944

1425 Enders JR, Mclean JA. 2009. Chiral and structural analysis of biomolecules using mass spectrometry
1426 and ion mobility - mass spectrometry. Chirality 21:E253-E264.
1427 Fenn LS, McLean JA. 2008. Enhanced carbohydrate structural selectivity in ion mobility-mass
1428 spectrometry analyses by boronic acid derivatization. Chem. Comm. 13:5505-5507
1429 Fernandez-Lima FA, Wei H, Gao YQ, Russell DH. 2009. On the structure elucidation using ion
1430 mobility spectrometry and molecular dynamics. J Phys Chem A 113:8221-8234.
1431 Fernández-Maestre R, Wu C, Hill Jr. HH. 2010. Using a buffer gas modifier to change separation
1432 selectivity in ion mobility spectrometry Int J Mass Spectrom 298:2-9.
1433 Fernandez-Maestre R, Harden CS, Ewing RG, Crawford CL, Hill Jr. HH. 2010. Chemical standards in
1434 ion mobility spectrometry. The Analyst.135:1433-1442
1435 Foloppe N, Chen I-J. 2009. Conformational sampling and energetics of drug-like molecules. Curr.
1436 Med Chem 16:3381-3413.
1437 Gehrke CW. 2001. Chromatography: a century of discovery 1900-2000: the bridge to the
1438 sciences/technology. Boca Raton, FL, USA: Elsevier.
1439 Gerlich D. 1992 In: State-Selected and State-to-State Ion-Molecule Reaction Dynamics. Part 1. Ng
1440 CY, Baer M, editors. LXXXII. John Wiley; New York: pp. 1–176
1441 Giles K, Wildgoose JL, Langridge DJ, Campuzano I. 2010. A method for direct measurement of ion
1442 mobilities using a travelling wave ion guide. Int J Mass Spectrom 298:10-16
1443 Giles K, Williams JP, Campuzano I. 2011. Enhancements in travelling wave ion mobility resolution.
1444 Rapid Comm Mass Spectrom 25:1559-1566.
1445 Gorshkov MP. 1982. Inventor's certificate USSR no. 966583 Byull Izobret 38.
1446 Griffin GW, Dzidic I, Carroll DI, Stillwell RN, Horning EC. 1973. Ion mass assignments based on
1447 mobility measuremets. validity of plasma chromatographic mass mobility correlations. Anal
1448 Chem 45:1204-1209.
1449 Guevremont R, Purves RW. 1999. Atmospheric pressure ion focusing in a high-field asymmetric
1450 waveform ion mobility spectrometer. Rev. Sci. Instrum. 70: 1370-1384
1451 Guo Y, Wang J, Javahery G, Thomson BA, Siu KWM. 2004. Ion Mobility Spectrometer with Radial
1452 Collisional Focusing. Anal. Chem. 77:266-275
1453 Guo Y, Srinivasan S, Gaiki S. 2009. Evaluation of the peak capacity of various rp-columns for small
1454 molecule compounds in gradient elution. Chromatographia 70:1045-1054.
1455 Hariharan CB, Baumbach JI, Vautz W. 2010. Linearized equations for the reduced ion mobilities of
1456 polar aliphatic organic compounds. Anal Chem 82:427-431.
1457 Harry EL, Reynolds JC, Bristow AWT, Wilson ID, Creaser CS. 2009. Direct analysis of pharmaceutical
1458 formulations from non-bonded reversed-phase thin-layer chromatography plates by
1459 desorption electrospray ionisation ion mobility mass spectrometry. Rapid Commun Mass
1460 Spectrom 23:2597-2604.
1461 Harry EL, Bristow AWT, Wilson ID, Creaser CS. 2011. Real-time reaction monitoring using ion
1462 mobility-mass spectrometry. Analyst 136:1728.
1463 Harvey SR, MacPhee CE, Barran PE, 2011. Ion mobility mass spectrometry for peptide analysis,
1464 Methods, 54, 4: 454-461
1465 Hatsis P, Brockman AH, Wu J-T. 2007. Evaluation of high-field asymmetric waveform ion mobility
1466 spectrometry coupled to nanoelectrospray ionization for bioanalysis in drug discovery. Rapid
1467 Commun Mass Spectrom 21:2295-2300.
1468 Heck AJR, van den Heuvel RHH. 2004. Investigation of intact protein complexes by mass
1469 spectrometry. Mass Spectrom Rev 23:368-389.
1470 von Helden G, Wyttenbach T, Bowers MT. 1995. Conformation of macromolecules in the gas phase:
1471 use of matrix-assisted laser desorption methods in ion chromatography. Science 267:1483-
1472 1485.
1473 Henderson SC, Valentine SJ, Counterman AE, Clemmer DE. 1999. Esi/ion trap/ion mobility/time-of-
1474 flight mass spectrometry for rapid and sensitive analysis of biomolecular mixtures. Anal Chem
1475 71:291-301.
1476 Hill CA, Thomas CLP. 2003. A pulsed corona discharge switchable high resolution ion mobility
1477 spectrometer-mass spectrometer. Analyst 128:55-60.
1478 Hoaglund-Hyzer CS, Counterman AE, Clemmer DE. 1999. Anhydrous protein ions. Chem Rev
1479 99:3037-3080.
1480 Hogan CJ, Ruotolo BT, Robinson CV, Fernandez de la Mora J. 2011. Tandem Differential Mobility
1481 Analysis-Mass Spectrometry Reveals Partial Gas-Phase Collapse of the GroEL ComplexJ.
1482 Phys. Chem. B.115:3614-3621

1483 Hogg AM, Kebarle P. 1965 Mass-Spectrometric Study of Ions at Near-Atmospheric Pressure. II.
1484 Ammonium Ions Produced by the Alpha Radiolysis of Ammonia and Their Solvation in the
1485 Gas Phase by Ammonia and Water Molecules. J. Chem. Phy. 43:449-457
1486 Holmes JL. 2006. Assigning structures to ions in the gas phase. New York: CRC Press.
1487 Homans SW. 2007. Water, water everywhere--except where it matters? Drug Discov Today 12:534-
1488 539.
1489 Howdle MD, Eckers C, Laures AM-F, Creaser CS. 2009. The use of shift reagents in ion mobility-
1490 mass spectrometry: studies on the complexation of an active pharmaceutical ingredient with
1491 polyethylene glycol excipients. J Am Soc Mass Spectrom 20:1-9.
1492 Howdle MD, Eckers C, Laures AM-F, Creaser CS. 2010. The effect of drift gas on the separation of
1493 active pharmaceutical ingredients and impurities by ion mobility-mass spectrometry. Int J
1494 Mass Spectrom 298:72-77.
1495 Huang MX, Markides KE, Lee ML. 1991. Evaluation of an ion mobility detector for supercritical fluid
1496 chromatography with solvent-modified carbon dioxide mobile phases. Chromatographia
1497 31:163-167.
1498 Ibrahim YM, Meot-Ner M, Alshraeh EH, El-Shall MS, Scheiner S. 2005. Stepwise hydration of ionized
1499 aromatics. energies, structures of the hydrated benzene cation, and the mechanism of
1500 deprotonation reactions. J Am Chem Soc 127:7053-7064.
1501 Jackson SN, Ugarov M, Egan T, Post JD, Langlais D, Schultz JA, Woods AS. 2007. Maldi-ion
1502 mobility-tofms imaging of lipids in rat brain tissue. J Mass Spectrom 42:1093-1098.
1503 Jafari MT, Khayamian T, Shaer V, Zarei N. 2007. Determination of veterinary drug residues in chicken
1504 meat using corona discharge ion mobility spectrometry. Anal Chim Acta 581:147-153.
1505 Jafari MT. 2006. Determination and identification of malathion, ethion and dichlorovos using ion
1506 mobility spectrometry. Talanta 69:1054-1058.
1507 Javahery G, Thomson B. 1997. A segmented radiofrequency-only quadrupole collision cell for
1508 measurements of ion collision cross section on a triple quadrupole mass spectrometer. J. Am.
1509 Soc. Mass Spectrom. 8:697-702
1510 Jarrold MF. 2000. Peptides and proteins in the vapor phase. Annu Rev Phys Chem 51:179-207.
1511 Jurneczko E, Barran PE. 2011. How useful is ion mobility mass spectrometry for structural biology?
1512 the relationship between protein crystal structures and their collision cross sections in the gas
1513 phase. Analyst 136:20.
1514 Kanu AB, Dwivedi P, Tam M, Matz L, Hill HH. 2008. Ion mobility-mass spectrometry. J. Mass
1515 Spectrom 43:1-22.
1516 Kaplan K, Graf S, Tanner C, Gonin M, Fuhrer K, Knochenmuss R, Dwivedi P, Hill HH. 2010. Resistive
1517 glass im-tofms. Anal Chem 82:9336-9343.
1518 Karasek FW, Hill HH, Kim SH. 1976. Plasma chromatography of heroin and cocaine with mass-
1519 identified mobility spectra. J Chromatogr 117:327-336.
1520 Karimi A, Alizadeh N. 2009. Rapid analysis of captopril in human plasma and pharmaceutical
1521 preparations by headspace solid phase microextraction based on polypyrrole film coupled to
1522 ion mobility spectrometry. Talanta 79:479-485.
1523 Karpas Z, Bell SE, Wang Y-F, Walsh M, Eiceman GA. 1994. The structure of protonated diamines
1524 and polyamines. Struct Chem 5:135-140.
1525 Karpas Z. 1991. The structure and mobility in air of protonated ketones. Int J Mass Spectrom
1526 107:435-440.
1527 Karpas Z. 1992. The mobility of protonated aminoalcohols: evidence for proton-induced cyclization.
1528 Struct Chem 3:139-141.
1529 Karpas Z, Berant Z, Shahal O. 1990. The effects of saturation and substitution on the mobility of
1530 protonated cyclic compounds. Int J Mass Spectrom Ion Proc 96:291-297.
1531 Karpas Z, Berant Z, Stimac RM. 1990. An ion mobility spectrometry/mass spectrometry (ims/ms)
1532 study of the site of protonation in anilines. Struct Chem 1:201-204.
1533 Karpas Z, Stimac RM, Rappoport Z. 1988. Differentiating between large isomers and derivation of
1534 structural information by ion mobility spectrometry / mass spectrometry techniques. Int J Mass
1535 Spectrom Ion Proc 83:163-175.
1536 Karpas Z, Tironi C. 1991. The mobility and ion structure of protonated aminoazoles. Struct Chem
1537 2:655-659.
1538 Kebarle P, Hogg AM. 1965. Mass-Spectrometric Study of Ions at Near Atmospheric Pressures. I. The
1539 Ionic Polymerization of Ethylene. The Journal of Chemical Physics. 42: 668-675
1540 Keller T, Keller A, Tutsch-Bauer E, Monticelli F. 2006. Application of ion mobility spectrometry in
1541 cases of forensic interest. Forensic Sci Int 161:130-140.

Kemper PR, Dupuis NF, Bowers MT. 2009. A new, higher resolution, ion mobility mass spectrometer. Int J Mass Spectrom 287:46-57.
Kinnear BS, Hartings MR, Jarrold MF. 2002. The energy landscape of unsolvated peptides: helix formation and cold denaturation in ac-a4g7a4 + h+. J Am Chem Soc 124:4422-4431.
Knapman TW, Berryman JT, Campuzano I, Harris SA, Ashcroft AE. 2010. Considerations in experimental and theoretical collision cross-section measurements of small molecules using travelling wave ion mobility spectrometry-mass spectrometry. Int J Mass Spectrom 298: 17-23.
Knutson E, Whitby K. 1975. Aerosol classification by electric mobility: Apparatus, theory, and applications. J. Aerosol Sci. 6 (6): 443–451Koeniger SL, Merenbloom SI, Clemmer DE. 2006. Evidence for many resolvable structures within conformation types of electrosprayed ubiquitin ions. J Phys Chem B 110:7017-7021.
Kolakowski BM, Mester Z. 2007. Review of applications of high-field asymmetric waveform ion mobility spectrometry (faims) and differential mobility spectrometry (dms). Analyst 132:842-864.
Krylov EV. 1999. A method of reducing diffusion losses in a drift spectrometer. Tech Phys+. 44:113-116
Krylov E, Nazarov EG, Miller RA, Tadjikov B, Eiceman GA. 2002. Field Dependence of Mobilities for Gas-Phase-Protonated Monomers and Proton-Bound Dimers of Ketones by Planar Field Asymmetric Waveform Ion Mobility Spectrometer (PFAIMS). J. Phys. Chem. A. 106:5437-5444
Krylov EV. 2003. Comparison of the planar and coaxial field asymmetrical waveform ion mobility spectrometer (FAIMS). Int. J. Mass Spectrom. 225:39-51
Krylov EV, Nazarov EG. 2009. Electric field dependence of the ion mobility. Int. J. Mass Spectrom. 285:149-156
Kurulugama RT, Nachtigall FM, Lee S, Valentine SJ, Clemmer DE. 2009. Overtone mobility spectrometry: part 1. experimental observations. J Am Soc Mass Spectrom 20:729-737.
Kwasnik M, Fernández FM. 2010. Theoretical and experimental study of the achievable separation power in resistive-glass atmospheric pressure ion mobility spectrometry. Rapid Commun Mas Spectrom 24:1911-1918.
Langevin P. 1905. Une formule fondamentale de théorie cinétique. Ann Chim Phys 5:245.
Lawrence AH. 1986. Ion mobility spectrometry/mass spectrometry of some prescription and illicit drugs. Anal Chem 58:1269-1272.
Levin DS, Vouros P, Miller RA, Nazarov EG, Morris JC. 2004. Characterization of Gas-Phase Molecular Interactions on Differential Mobility Ion Behavior Utilizing an Electrospray Ionization-Differential Mobility-Mass Spectrometer System. Anal. Chem.78: 96-106
Levin DS, Vouros P, Miller RA, Nazarov EG. 2007. Using a nanoelectrospray-differential mobility spectrometer-mass spectrometer system for the analysis of oligosaccharides with solvent selected control over esi aggregate ion formation. J Am Soc Mass Spectrom 18:502-511
Li X, Stoll DR, Carr PW. 2009. Equation for peak capacity estimation in two-dimensional liquid chromatography. Anal Chem 81:845-850.
Likar MD, Cheng G, Mahajan N, Zhang Z. 2011. Rapid identification and absence of drug tests for ag-013736 in 1 mg axitinib tablets by ion mobility spectrometry and dart(tm) mass spectrometry. J Pharm Biomed Anal 55:569-573.
Lipinski CA, Lombardo F, Dominy BW, Feeney PJ. 1997. Experimental and computational approaches to estimate solubility and permeability in drug discovery and development settings. Adv Drug Del Rev 23:3-25.
Liu H, Yao X, Liu M, Hu Z, Fan B. 2007a. Prediction of gas-phase reduced ion mobility constants (k(0)) based on the multiple linear regression and projection pursuit regression. Talanta 71:258-263.
Liu X, Valentine SJ, Plasencia MD, Trimpin S, Naylor S, Clemmer DE. 2007b. Mapping the human plasma proteome by scx-lc-ims-ms. J Am Soc Mass Spectrom 18:1249-1264.
Maitra U, Bag BG, Rao P, Powell D. 1995. Asymmetric synthesis of steroidal Troger's base analogues. X-ray molecular structure of methyl 3α,12α-{6H,12H-5,11-methanodibenzo[b,f][1,5]diazocine-2,8-bisacetoxy}-5β-cholan-24-oate. J. Chem. Soc. Perkin Trans. 1:2049
Manard MJ, Trainham R, Weeks S, Coy SL, Crylov EV, Nazarov EG. 2010. Differential mobility spectrometry/mass spectrometry: The design of a new mass spectrometer for real-time chemical analysis in the field. Int J Mass Spectrom 295: 138-144
Mao Y, Ratner MA, Jarrold MF. 2001. Molecular dynamics simulations of the rehydration of folded and unfolded cytochrome c ions in the vapor phase. J Am Chem Soc 123:6503-6507.

1600 Martínez-Lozano P, Rus J. 2010. Separation of Isomers L-Alanine and Sarcosine in Urine by
1601 Electrospray Ionization and Tandem Differential Mobility Analysis-Mass Spectrometry. J Am
1602 Soc Mass Spectrom. 21(7): 1129-1132
1603 Martínez-Lozano P, Criado E, Vidal G, Cristoni S, Franzoso F, Piatti M, Brambilla P. 2011. Differential
1604 mobility analysis-mass spectrometry coupled to XCMS algorithm as a novel analytical
1605 platform for metabolic profiling. Metabolomics. 1-14
1606 Mason EA, McDaniel EW, 1988. Transport Properties of Ions in Gases, New York: John Wiley & Sons,
1607 560p
1608 Matz LM, Hill HH. 2002a. Evaluating the separation of amphetamines by electrospray ionization ion
1609 mobility spectrometry/ms and charge competition within the ESI process. Anal Chem 74:420-
1610 427.
1611 Matz LM, Hill HH, Beegle LW, Kanik I. 2002b. Investigation of drift gas selectivity in high resolution ion
1612 mobility spectrometry with mass spectrometry detection. J Am Soc Mass Spectrom 13:300-
1613 307.
1614 McAfee KB, Edelson D. 1963. Identification and mobility of ions in a Townsend discharge by time-
1615 resolved mass spectrometry. Proc Phys Soc 81:382-384.
1616 McDaniel EW, Martin DW. 1960. Drift tube-mass spectrometer for studies of thermal-energy ion-
1617 molecule reactions. Technical Report no. 3.
1618 Mie A, Jörntén-Karlsson M, Axelsson B-O, Ray A, Reimann CT. 2007. Enantiomer separation of
1619 amino acids by complexation with chiral reference compounds and high-field asymmetric
1620 waveform ion mobility spectrometry: preliminary results and possible limitations. Anal Chem
1621 79:2850-2858.
1622 Milloy HB, Crompton RW. 1977. Momentum-transfer cross section for electron-helium collisions in the
1623 range 4-12 ev. Phys Rev A 15:1847.
1624 Momoh PO, El-Shall MS. 2008. Gas phase hydration of organic ions. Phys Chem Chem Phys
1625 10:4827.
1626 Myung S, Lee YJ, Moon MH, Taraszka J, Sowell R, Koeniger S, Hilderbrand AE, Valentine SJ,
1627 Cherbas L, Cherbas P, Kaufmann TC, Miller DF, Mechref Y, Novotny MV, Ewing MA,
1628 Sporleder CR, Clemmer DE. 2003. Development of high-sensitivity ion trap ion mobility
1629 spectrometry time-of-flight techniques: a high-throughput nano-lc-ims-tof separation of
1630 peptides arising from a drosophila protein extract. Anal Chem 75:5137-5145.
1631 Nazarov EG, Coy SL, Krylov EV, Miller RA, Eiceman GA. 2006. Pressure Effects in Differential
1632 Mobility Spectrometry. Anal. Chem. 78: 7697-7706
1633 O'Donnell RM, Sun X, Harrington P de B. 2008. Pharmaceutical applications of ion mobility
1634 spectrometry. Trac Trends Anal. Chem. 27:44-53.
1635 Pace CN, Treviño S, Prabhakaran E, Scholtz JM. 2004. Protein structure, stability and solubility in
1636 water and other solvents. Philos Trans Royal Soc (London) B Biol Sci 359:1225-1234;.
1637 Poornima CS, Dean PM. 1995. Hydration in drug design. 1. multiple hydrogen-bonding features of
1638 water molecules in mediating protein-ligand interactions. J computer-aided mol des 9:500-512.
1639 Poully J-C, Nieuwjaer N, Pierre Schermann J. 2008. Structure and dynamics of molecules of
1640 pharmaceutical interest in gas phase and in aqueous phase. Phys. Scr 78:058123.
1641 Prieto M, Yost RA. 2011. Spherical FAIMS: comparison of curved electrode geometries. Int. J Ion
1642 Mobil. Spec.14: 61-69
1643 Pringle SD, Giles K, Wildgoose JL, Williams JP, Slade SE, Thalassinos K, Bateman RH, Bowers MT,
1644 Scrivens JH. 2007. An investigation of the mobility separation of some peptide and protein ions using
1645 a new hybrid quadrupole/travelling wave IMS/oa-ToF instrument. Int. J. Mass Spectrom. 261:1–12.
1646 Pris AD, Mondello FJ, Wroczynski RJ, Murray AJ, Boudries H, Surman CM, Paxon TL. 2009.
1647 Improved specific biodetection with ion trap mobility spectrometry (itms): a 10-min, multiplexed,
1648 immunomagnetic elisa. Anal Chem 81:9948-9954.
1649 Purves RW, Barnett DA, Ells B, Guevremont R. 2000. Investigation of bovine ubiquitin conformers
1650 separated by high-field asymmetric waveform ion mobility spectrometry: cross section
1651 measurements using energy-loss experiments with a triple quadrupole mass spectrometer. J
1652 Am Soc Mass Spectrom. 11:738-745
1653 Shvartsburg A, Purves RW. 2010., differential ion mobility spectrometry: nonlinear ion transport and
1654 fundamentals of faims, crc press, taylor and francis group, boca raton, fl 33487-2742, usa
1655 (2009) ISBN 978-1-4200-5106-3 hardcover, 322 pp. J Am Soc Mass Spectrom 21:R3-R3.
1656 Rand KD, Pringle SD, Murphy JP, Fadgen KE, Brown J, Engen JR. 2009. Gas-phase
1657 hydrogen/deuterium exchange in a traveling wave ion guide for the examination of protein
1658 conformations. Anal Chem 81:10019-10028.

1659 Révész Á, Schröder D, Rokob TA, Havlík M, Dolenský B. 2011. In - flight epimerization of a
1660 *bis* - Tröger base. Angew Chem Int Ed 50:2401-2404.
1661 Roentgen W. 1896. Eine neue art von strahlen 4th ed. Würzburg: Stahel'schen K.B. Hof und
1662 Universitätsbuch und Kunsthandlung.
1663 Ruotolo BT, Giles K, Campuzano I, Sandercock AM, Bateman RH, Robinson CV. 2005. Evidence for
1664 macromolecular protein rings in the absence of bulk water. Science 310:1658-1661.
1665 Ruotolo BT, Gillig KJ, Stone EG, Russell DH. 2002a. Peak capacity of ion mobility mass spectrometry:
1666 separation of peptides in helium buffer gas. J Chromatog B 782:385-392.
1667 Ruotolo BT, Gillig KJ, Stone EG, Russell DH, Fuhrer K, Gonin M, Schultz JA. 2002b. Analysis of
1668 protein mixtures by matrix-assisted laser desorption ionization-ion mobility-orthogonal-time-of-
1669 flight mass spectrometry. Int J Mass Spectrom 219:253-267.
1670 Rus J, Moro D, Sillero JA, Royuela J, Casado A, Estevez-Molinero F, Fernández de la Mora J. 2010.
1671 IMS–MS studies based on coupling a differential mobility analyzer (DMA) to commercial API–
1672 MS systems. Int J Mass Spectrom. 298:30-40
1673 Rutherford E. 1897. The velocity and rate of recombination of the ions of gases exposed to röntgen
1674 radiation. Philosophical Magazine 5: 44:422.
1675 Santos LFA, Iglesias AH, Pilau EJ, Gomes AF, Gozzo FC. 2010. Traveling-wave ion mobility mass
1676 spectrometry analysis of isomeric modified peptides arising from chemical cross-linking. J Am
1677 Soc Mass Spectrom 21:2062-2069.
1678 Schneider BB, Covey TR, Coy SL, Krylov EV, Nazarov EG. 2010a. Planar differential mobility
1679 spectrometer as a pre-filter for atmospheric pressure ionization mass spectrometry. Int J
1680 Mass Spectrom. 298: 45-54
1681 Schneider BB, Covey TR, Coy SL, Krylov EV, Nazarov EG. 2010b. Chemical effects in the separation
1682 process of a differential mobility/mass spectrometer system. Anal Chem 82:1867-1880.
1683 Schneider BB, Covey TR, Coy SL, Krylov EV, Nazarov EG. 2010c. Control of chemical effects in the
1684 separation process of a differential mobility mass spectrometer system Eur J Mass Spectrom
1685 16: 57-71
1686 Schultz SG, Solomon AK. 1961. Determination of the effective hydrodynamic radii of small molecules
1687 by viscometry. J Gen Physiol 44:1189 -1199.
1688 Shelimov KB, Clemmer DE, Hudgins RR, Jarrold MF. 1997. Protein structure *in vacuo*: gas-phase
1689 conformations of bpti and cytochrome c. J Am Chem Soc 119:2240-2248.
1690 Shelimov KB, Jarrold MF. 1997. Conformations, unfolding, and refolding of apomyoglobin in vacuum:
1691 an activation barrier for gas-phase protein folding. J Am Chem Soc 119:2987-2994.
1692 Shvartsburg AA, Clemmer DE, Smith RD. 2010a. Isotopic effect on ion mobility and separation of
1693 isotopomers by high-field ion mobility spectrometry. Anal Chem 82:8047-8051.
1694 Shvartsburg AA, Danielson WF, Smith RD. 2010b. High-resolution differential ion mobility separations
1695 using helium-rich gases. Anal Chem 82:2456-2462.
1696 Shvartsburg AA, Jarrold MF. 1996. An exact hard-spheres scattering model for the mobilities of
1697 polyatomic ions. Chem Phys Lett 261:86-91.
1698 Shvartsburg AA, Mashkevich SV, Baker ES, Smith RD. 2007. Optimization of algorithms for ion
1699 mobility calculations. J Phys Chem A 111:2002-2010.
1700 Shvartsburg AA, Smith RD. 2008. Fundamentals of traveling wave ion mobility spectrometry. Anal
1701 Chem 80:9689-9699.
1702 Shvartsburg AA, Smith RD, Wilks A, Koehl A, Ruiz-Alonso D, Boyle B. 2009a. Ultrafast differential ion
1703 mobility spectrometry at extreme electric fields in multichannel microchips. Anal Chem
1704 81:6489-6495.
1705 Shvartsburg AA, Tang K, Smith RD. 2004. Modeling the resolution and sensitivity of faims analyses. J
1706 Am Soc Mass Spectrom 15:1487-1498.
1707 Shvartsburg AA, Tang K, Smith RD, Holden M, Rush M, Thompson A, Toutoungi D. 2009b. Ultrafast
1708 differential ion mobility spectrometry at extreme electric fields coupled to mass spectrometry.
1709 Anal Chem 81:8048-8053.
1710 Siems WF, Wu C, Tarver EE, Hill HHJ, Larsen PR, McMinn DG. 1994. Measuring the resolving power
1711 of ion mobility spectrometers. Anal Chem 66:4195-4201.
1712 Siu C-K, Guo Y, Saminathan IS, Hopkinson AC, Siu KWM. 2010. Optimization of parameters used in
1713 algorithms of ion-mobility calculation for conformational analyses. J Phys Chem B 114:1204-
1714 1212.
1715 Smith DP, Knapman TW, Campuzano I, Malham RW, Berryman JT, Radford SE, Ashcroft AE. 2009a.
1716 Deciphering drift time measurements from travelling wave ion mobility spectrometry-mass
1717 spectrometry studies. Eur J Mass Spectrom 15:113-130.

Smith RD, Prasad S, Tang K, Manura D, Papanastasiou D. 2009b. Simulation of ion motion in faims through combined use of simion and modified sds. Anal. chem. 81:8749-8757.
Snyder AP, Blyth DA, Parsons JA. 1996. Ion mobility spectrometry as an immunoassay detection technique. J Microbiol Meth 27:81-88.
Snyder AP, Harden CS, Brittain AH, Kim MG, Arnold NS, Meuzelaar HLC. 1993. Portable hand-held gas chromatography/ion mobility spectrometry device. Anal Chem 65:299-306.
Souza Pessôa G de, Pilau EJ, Gozzo FC, Zezzi Arruda MA. 2011. Ion mobility mass spectrometry: an elegant alternative focusing on speciation studies. J. Anal At Spectrom 26:201.
Steiner WE, English WA, Hill HH. 2006.Ion−Neutral Potential Models in Atmospheric Pressure Ion Mobility Time-of-Flight Mass Spectrometry IM(tof)MSJ. Phys. Chem. A. 110:1836-1844
Stolzenburg M, McMurry P. 2008. Equations Governing Single and Tandem DMA Configurations and a New Lognormal Approximation to the Transfer Function. Aerosol Sci. Tech. 42, 421-432Tabrizchi M, Jazan E. 2010. Inverse ion mobility spectrometry. Anal Chem 82:746-750.
Tang K, Shvartsburg AA, Lee H-N, Prior DC, Buschbach MA, Li F, Tolmachev AV, Anderson GA, Smith RD. 2005. High-sensitivity ion mobility spectrometry/mass spectrometry using electrodynamic ion funnel interfaces. Anal Chem 77:3330-3339.
Tang X, Bruce JE, Hill HH. 2006. Characterizing electrospray ionization using atmospheric pressure ion mobility spectrometry. Anal Chem 78:7751-7760.
Taraszka JA, Gao X, Valentine SJ, Sowell RA, Koeniger SL, Miller DF, Kaufman TC, Clemmer DE. 2005. Proteome profiling for assessing diversity: analysis of individual heads of drosophila melanogaster using lc−ion mobility−ms. J Proteome Res 4:1238-1247.
Tarver EE. 2004. External second gate, fourier transform ion mobility spectrometry: parametric optimization for detection of weapons of mass destruction. Sensors 4:1-13.
Thalassinos K, Grabenauer M, Slade SE, Hilton GR, Bowers MT, Scrivens JH. 2009. Characterization of phosphorylated peptides using travelling wave-based and drift cell ion mobility mass spectrometry. Anal Chem 81:248-254.
Thomson JJ. 1903. Conduction of electricity through gases. Nature 69:74-75.
Thomson JJ, Rutherford E. 1896. On the passage of electricity through gases exposed to röntgen rays. Phil Mag Series 5 42:392.
Tuovinen K, Paakkanen H, Hänninen O. 2000. Detection of pesticides from liquid matrices by ion mobility spectrometry. Anal Chim Acta 404:7-17.
Turner RB, Brokenshire JL. 1994. Hand-held ion mobility spectrometers. Trac Trends Anal Chem 13:281-286.
Ude S, Fernández de la Mora J, Thomson BA. 2004. Charge-Induced Unfolding of Multiply Charged Polyethylene Glycol Ions. J. Am. Chem. Soc.126: 12184-12190
Uetrecht C, Rose RJ, Duijn E van, Lorenzen K, Heck AJR. 2010. Ion mobility mass spectrometry of proteins and protein assemblies. Chem Soc Rev 39:1633-1655.
Valentine SJ, Kulchania M, Barnes CAS, Clemmer DE. 2001. Multidimensional separations of complex peptide mixtures: a combined high-performance liquid chromatography/ion mobility/time-of-flight mass spectrometry approach. Int J Mass Spectrom 212:97-109.
Valentine SJ, Stokes ST, Kurulugama RT, Nachtigall FM, Clemmer DE. 2009. Overtone mobility spectrometry: part 2. theoretical considerations of resolving power. J Am Soc Mass Spectrom 20:738-750.
Vautz W, Schwarz L, Hariharan C, Schilling M. 2010. Ion characterisation by comparison of ion mobility spectrometry and mass spectrometry data. Int J Ion Mobil Spec 13:121-129.
Vonderach M, Ehrler OT, Weis P, Kappes MM. 2011. Combining ion mobility spectrometry, mass spectrometry, and photoelectron spectroscopy in a high-transmission instrument. Anal Chem 83:1108-1115.
Wang B, Valentine S, Plasencia M, Raghuraman S, Zhang X. 2010. Artificial neural networks for the prediction of peptide drift time in ion mobility mass spectrometry. BMC Bioinfo 11:182.
Wang Y, Nacson S, Pawliszyn J. 2007. The coupling of solid-phase microextraction/surface enhanced laser desorption/ionization to ion mobility spectrometry for drug analysis. Anal Chim Acta 582:50-54.
Wessel MD, Jurs PC. 1994. Prediction of reduced ion mobility constants from structural information using multiple linear regression analysis and computational neural networks. Anal Chem 66:2480-2487.
Wessel MD, Sutter JM, Jurs PC. 1996. Prediction of reduced ion mobility constants of organic compounds from molecular structure. Anal Chem 68:4237-4243.

Weston DJ, Bateman R, Wilson ID, Wood TR, Creaser CS. 2005. Direct analysis of pharmaceutical drug formulations using ion mobility spectrometry/quadrupole-time-of-flight mass spectrometry combined with desorption electrospray ionization. Anal. Chem 77:7572-7580.

Weston DJ. 2010. Ambient ionization mass spectrometry: current understanding of mechanistic theory; analytical performance and application areas. Analyst 135:661.

Williams JP, Lough JA, Campuzano I, Richardson K, Sadler PJ. 2009a. Use of ion mobility mass spectrometry and a collision cross-section algorithm to study an organometallic ruthenium anticancer complex and its adducts with a dna oligonucleotide. Rapid Commun Mass Spectrom 23:3563-3569.

Williams JP, Bugarcic T, Habtemariam A, Giles K, Campuzano I, Rodger PM, Sadler PJ. 2009b. Isomer separation and gas-phase configurations of organoruthenium anticancer complexes: ion mobility mass spectrometry and modeling. J Am Soc Mass Spectrom 20:1119-1122.

Williams JP, Grabenauer M, Holland RJ, Carpenter CJ, Wormald MR, Giles K, Harvey DJ, Bateman RH, Scrivens JH, Bowers MT. 2010. Characterization of simple isomeric oligosaccharides and the rapid separation of glycan mixtures by ion mobility mass spectrometry. Int J Mass Spectrom 298:119-127.

Wren SAC. 2005. Peak capacity in gradient ultra performance liquid chromatography (uplc). J Pharm Biomed Anal 38:337-343.

Wright P, Alex A, Nyaruwata T, Parsons T, Pullen FS. (2010). Using density functional theory to rationalise the mass spectral fragmentation of maraviroc and its metabolites. Rapid Commun in Mass Spectrom, 24: 1025–1031

Wu C, Siems WF, Asbury GR, Hill HH. 1998. Electrospray ionization high-resolution ion mobility spectrometry−mass spectrometry. Anal Chem 70:4929-4938.

Wyttenbach T, Kemper PR, Bowers MT. 2001. Design of a new electrospray ion mobility mass spectrometer. Int J Mass Spectrom 212:13-23.

Wyttenbach T, Paizs B, Barran P, Breci L, Liu D, Suhai S, Wysocki VH, Bowers MT. 2003. The effect of the initial water of hydration on the energetics, structures, and h/d exchange mechanism of a family of pentapeptides: an experimental and theoretical study. J Am Chem Soc 125:13768-13775.

Zhao W, Bhushan A, Schivo M, Kenyon NJ, Davis CE. 2010. Miniature differential mobility spectrometry (dms) advances towards portable autonomous health diagnostic systems. In: Wearable and autonomous biomedical devices and systems for smart environment. Springer Berlin Heidelberg. Lecture Notes in Electrical Engineering Vol. 75, p. 55-73. http://dx.doi.org/10.1007/978-3-642-15687-8_3.

Zhou M, Robinson CV. 2010. When proteomics meets structural biology. Trends Biochem Sci 35:522-529.

Zhu M, Bendiak B, Clowers B, Hill HH. 2009. Ion mobility-mass spectrometry analysis of isomeric carbohydrate precursor ions. Anal Bioanal Chem 394:1853-1867.

Zolotov YA. 2006. Ion mobility spectrometry. J Anal Chem 61:519-519.